Original Article

MOLECULAR METABOLISM

Loss of mitochondrial pyruvate carrier 1 supports proline-dependent proliferation and collagen biosynthesis in ovarian cancer

M. Rufaik Farook[1], Zack Croxford[1], Steffan Morgan[1], Anthony D. Horlock[1], Amy K. Holt[3], April Rees[1], Benjamin J. Jenkins[1], Carmen Tse[1], Emma Stanton[1], D. Mark Davies[1,2], Catherine A. Thornton[1], Nicholas Jones[1], I. Martin Sheldon[1], Emma E. Vincent[3], James G. Cronin[1,*]

ABSTRACT

The pyruvate transporter MPC1 (mitochondrial pyruvate carrier 1) acts as a tumour-suppressor, loss of which correlates with a pro-tumorigenic phenotype and poor survival in several tumour types. In high-grade serous ovarian cancers (HGSOC), patients display copy number loss of *MPC1* in around 78% of cases and reduced *MPC1* mRNA expression. To explore the metabolic effect of reduced expression, we demonstrate that depleting *MPC1* in HGSOC cell lines drives expression of key proline biosynthetic genes; *PYCR1*, *PYCR2* and *PYCR3,* and biosynthesis of proline. We show that altered proline metabolism underpins cancer cell proliferation, reactive oxygen species (ROS) production, and type I and type VI collagen formation in ovarian cancer cells. Furthermore, exploring The Cancer Genome Atlas, we discovered the *PYCR3* isozyme to be highly expressed in a third of HGSOC patients, which was associated with more aggressive disease and diagnosis at a younger age. Taken together, our study highlights that targeting proline metabolism is a potential therapeutic avenue for the treatment of HGSOC.

Keywords Proline; High grade serous ovarian cancer; *PYCR1*; *PYCR2*; *PYCR3*; Mitochonrial pyruvate carrier; Pyrroline-5-carboxylate reductase; Oncometabolism; Collagen

1. INTRODUCTION

High-grade serous ovarian cancer (HGSOC) is the leading cause of death from gynaecological cancer [1,2]. The is due in part to late-stage diagnosis, at which point disease is often widely metastatic in the abdomen, resulting in a 10-year survival rate of only 15% [3,4]. Most patients initially respond well to chemotherapy and attain complete remission; however, relapse is common and the majority of patients experience chemotherapy-resistant disease within 18-months of initial treatment, making HGSOC an important clinical challenge [2,5]. Despite recent promising therapeutic developments, treating late-stage HGSOC is rarely curative, and serves only to delay disease recurrence. Thus, new targets and therapies are urgently needed to better treat this aggressive and therapy-resistant disease.

Metabolic reprogramming, now an established hallmark of cancer, has historically, focussed on the contribution of glycolytic and tricarboxylic acid (TCA) cycle pathway activity to support tumorigenesis. Although, more recently the contribution of amino acids as energy sources and in the maintenance of cancer cell redox balance has come to the fore [6]. Cancer cells rewire metabolic pathways to meet the high energy demands of tumour development, whilst producing the macromolecules required for cell proliferation and survival. Thus, targeting cancer metabolism has been extensively explored, but can be challenging. For instance, metabolic flexibility in ovarian cancer has been shown to drive tumour progression and resistance to therapy [7—11].

Glucose is the primary source of carbon for generating the energy and biosynthetic intermediates required for sustained growth and cell survival [12]. Glucose-derived pyruvate, generated via glycolysis, is transported into mitochondria via the mitochondrial pyruvate carrier protein complex (MPC1 and MPC2), providing the major pool of acetyl-CoA for oxidative metabolism [13,14]. Paradoxically, *MPC1* is under-expressed or deleted in multiple cancers, which correlates with poor prognoses [15,16]. In HGSOC, around 78% of cases display copy number loss of *MPC1* (The Cancer Genome Atlas; TCGA) and overall, a reduced expression of *MPC1* [17]. Cancer cells may compensate for disrupted transport of pyruvate into mitochondria by rerouting glutamine metabolism to generate oxaloacetate (OAA) and acetyl-CoA to sustain the tricarboxylic acid (TCA) cycle [18]. A shift to metabolic dependence on glutamine also drives resistance to chemotherapy in ovarian cancer [19,20]. Accordingly, ovarian cancers become reliant on glutamine for cell survival, tumour growth, invasion, metastasis, and therapy-resistance [19,21].

Glutamine is also metabolised via the pyrroline-5-carboxylate reductase (PYCR) isozymes, which provide the carbon and nitrogen required

[1]Institute of Life Science, Swansea University Medical School, Faculty of Medicine, Health & Life Science, Swansea University, Swansea, SA2 8PP, United Kingdom [2]Department of Oncology, South-West Wales Cancer Centre, Singleton Hospital, Swansea SA2 8QA, UK [3]School of Translational Health Sciences, Dorothy Hodgkin Building, University of Bristol, Bristol, BS1 3NY, UK

*Corresponding author. E-mail: J.Cronin@Swansea.ac.uk (J.G. Cronin).

Received June 16, 2023 • Revision received February 2, 2024 • Accepted February 9, 2024 • Available online 13 February 2024

https://doi.org/10.1016/j.molmet.2024.101900

by cancer cells for proline-dependent cellular processes [22–26]. Proline is particularly important for cellular energy metabolism, redox balance, and the production of the extracellular matrix (ECM) protein collagen [22,26–30]. Furthermore, anchorage-independent induced accumulation and secretion of proline supports increased production of collagen in cancer cells [31]. Ovarian cancer cells deposit type VI collagen during tumour formation, a factor found to contribute to therapy resistance [32–34]. Breast cancer cells have also been found to be dependent on extracellular pyruvate for collagen-based remodelling of the ECM in the lung metastatic niche [35], suggesting there may be promise in targeting collagen biosynthesis and remodelling for treatment of late-stage disease.

In this study we sought to determine whether dysregulated pyruvate metabolism in ovarian cancer, due to reduced *MPC1*, drives collagen deposition and ECM formation. We demonstrate that depletion of *MPC1* causes accumulation of intracellular pyruvate and increased expression of proline biosynthesis genes, which were demonstrated to be critical for ovarian cancer cell proliferation and colony formation. Furthermore, we show that altered proline metabolism underpins cancer cell proliferation, reactive oxygen species (ROS) production, and type I and type VI collagen formation in ovarian cancer cells. Consistent with this, TCGA data obtained for HGSOC patients demonstrated copy number gain of the chromosomal region containing the *PCYR3* locus in 92% of HGSOC patients, with 1 in 3 patients displaying mRNA amplification of *PYCR3*. In summary, we provide a mechanistic understanding underlying the role of *MPC1* in ovarian cancer; coupling dysregulated pyruvate metabolism to the metabolic reprogramming of proline biosynthesis and collagen formation that may underpin ovarian cancer progression and therapy resistance.

2. MATERIALS AND METHODS

2.1. Cell culture

The PEO1 (#10032308) and PEO4 (#10032309) cell lines were purchased from the European Collection of Authenticated Cell Cultures, England. The OVCAR3 (#HTB-161) cell line was purchased from American Type Culture Collection, England. PEO1, PEO4 and OVCAR3 cell lines have previously been phenotypically and genotypically characterised as representative of HGSOC [36,37]. For routine culture, PEO1 and PEO4 cells were maintained in RPMI 1640 growth medium (#31870, Thermo Fisher Scientific, UK), supplemented with 10% foetal bovine serum (FBS) (#FB-1550, Biosera, USA), 2 mM glutamine (#25030081, Thermo Fisher Scientific, UK), 1% antibacterial antimycotic solution (ABAM) (#A5955, Merck, UK). For routine culture, OVCAR3 cells were maintained in RPMI 1640 growth medium supplemented with 20% FBS (#FB-1550, Biosera, USA), 2 mM glutamine, 0.1% insulin (#I0516, Merck) and 1% ABAM (#A5955, Merck). All cells were cultured in TC treated Corning® T-25 (#CLS430639, Merck), T-75 (#CLS430641U, Merck), or T-175 (#CLS431080, Merck) cell culture flasks and incubated at 37 °C in a humidified 5% CO_2 chamber. Growth medium was replaced every 2–3 days and cells were subcultured, using Accutase® cell detachment solution (#SCR005, Sigma–Aldrich), to ensure 70–80% confluency.

2.2. Small molecule inhibitors

To inhibit pyruvate transport into mitochondria UK5099 (#4186. Tocris, UK), a potent inhibitor for MPC1, was used. Cell lines PEO1, PEO4 or OVCAR3 were seeded at 2×10^4 cells per 100 μl per well in a 96-well plate. After 24 h, media were replaced with vehicle control (Dimethyl sulfoxide; DMSO, #D8418, Merck) or UK5099 inhibitor at concentrations of 2.5 μM or 5 μM. Each condition had a minimum of 4 technical replicates and experiments were repeated on at least three separate occasions with independent cell passages.

To determine the effect of glutamine or proline on cell proliferation in the presence of UK5099, high glucose DMEM media without glutamine, phenol red or sodium pyruvate (#31053044, Thermo Fisher Scientific) was mixed with DMEM media without glucose, glutamine, phenol red or sodium pyruvate (#A1443001, Thermo Fisher Scientific) to achieve 11.1 mM glucose serum-free growth media. Then, 10,000 cells/well in 200 μl media were seeded in a 96-well plate with five technical replicate wells for each condition in DMEM media (20% FBS) with 2 mM glutamine and no proline; DMEM media (20% FBS) without glutamine and proline; or DMEM media (20% FBS) with 2 mM proline but no glutamine. The 96-well plate was further incubated for 16 h at 37 °C and 5% CO_2. Following the incubation, media was aspirated, and cells were briefly washed with 200 μl of PBS. Plates were immediately frozen at −80 °C before performing the CyQUANT assay. The CyQUANT cell proliferation assay kit was used to quantify DNA content following the manufacturer's protocol (#C7026, Thermo Fisher Scientific). Briefly, the cell supernatants were carefully aspirated, and cells were gently washed with 100 μl of ice-cold PBS. The plate was then stored at −80 °C for a minimum of 4 h. Prior to making up the CyQUANT GR solution, the plate was thawed to room temperature. Then 200 μl of CyQUANT GR buffer was added to each sample well. The plate was wrapped in aluminium foil and incubated for 20 min at room temperature with gentle agitation. A λDNA standard curve was generated in duplicate in a new 96-well clear bottom black plate (#CLS3603, Sigma–Aldrich). The CyQUANT GR samples were then transferred to the new 96-well clear bottom black plate. The fluorescence was measured using POLARstar Omega plate reader (BMG Labtech, Ortenberg, Germany) at 480 nm excitation and 520 nm emission range and DNA concentrations extrapolated from the λDNA standard curve.

2.3. Metabolic assays

Extracellular glucose concentrations were determined using the glucose assay kit 1 (#1200032002, Eton Bioscience, USA), and absorbance measured at 490 nm; Extracellular pyruvate concentrations were determined using the pyruvate assay kit (#1200041002, Eton Bioscience), and absorbance was measured at 570 nm; Extracellular glutamine was determined using the Glutamine assay kit (#ab197011, Abcam, Cambridge, UK), and absorbance was measured at 450 nm; Extracellular L-lactate concentrations were determined using the L-Lactate Assay Kit (#MAK329, Merck), and absorbance was measured at 565 nm.

All assays were performed according to manufacturer's instructions and absorbance readings were measured using a POLARstar Omega microplate reader (BMG Labtech). Metabolite concentrations were extrapolated from a linear regression fit of known standards, and then normalised to CyQUANT data (ng/ml DNA) to account for any differences in the number of cells.

2.4. Immunoblotting

Cell proteins were isolated using PhosphoSafe™ Extraction Reagent (#71296; Merck). Protein lysates (10 μg) were solubilized by boiling for 5 min in Laemmli loading buffer (#S3401-10VL, Merck) and separated using SDS-polyacrylamide gel electrophoresis. The proteins were transferred to a 0.2 μm polyvinylidene difluoro membrane (PVDF) (Millipore, Watford, UK), using the Trans-Blot Turbo semi-dry transfer system (Bio-Rad, UK). The membranes were then blocked for 1 h using SuperBlock Blocking Buffer (#37537, Thermo Fisher Scientific). Membranes were probed overnight at 4 °C with primary antibodies to

MPC1 (RRID: AB_2773729, #14462, Cell Signaling Technology (CST), Danvers, MA, USA), MPC2 (RRID: AB_2799295, #46141, CST), Hexokinase 1 (HK1; RRID:AB_2116996, #2024, CST), Hexokinase 2 (HK2; RRID:AB_2232946, #2867, CST), Pyruvate kinase M2 (PKM2; RRID:AB_1904096, #4053, CST), Pyruvate dehydrogenase (PDH; RRID:AB_2162926, #3205, CST), Lactate dehydrogenase A (LDHA; RRID:AB_2066887, #3582, CST), Phosphofructokinase A (PFKP; RRID:AB_2713957, #8164, CST), Glucose-6-phosphate dehydrogenase (G6PD; RRID:AB_2797861, #12263, Cell Signaling), c-Myc (RRID:AB_1903938, #5605, CST), TP53 Induced Glycolysis Regulatory Phosphatase (TIGAR; RRID:AB_1249512, #sc-74577, Santa Cruz Biotechnology) or Collagen VI (RRID:AB_2847919, #ab182744, Abcam), diluted in 5% BSA (w/v) or 5% non-fat milk (w/v) in TBS-T, according to each antibody's datasheet. After three 5 min washes in TBS-T, membranes were incubated for 1 h with 1:1000 dilution HRP-linked anti-rabbit IgG (RRID:AB_2099233, #7074, CST) or anti-mouse IgG (RRID:AB_330924, #7076, CST).

Protein reactivity was assessed by enhanced chemiluminescent, Immobilon® ECL Ultra Western HRP Substrate (#WBULS0100, Merck, UK). Membranes were analysed on the ChemiDoc XRS system (Bio-Rad, UK) to acquire images for further analysis, ensuring protein bands did not reach saturation. Densitometry of western blot bands was determined using Quantity One version 4.6.3 software (Bio-Rad, UK). After imaging, membranes were stripped for 30 min with Restore Western Blot Stripping Buffer (#10057103, Thermo Fisher Scientific) and re-probed with another primary antibody, or with 1:1000 dilution anti-mouse β-actin (RRID:AB_2242334, #3700, CST), anti-rabbit β-actin (RRID:AB_10899528, #ab115777; Abcam, UK) or VDAC (RRID:AB_2272627, #4866, CST). Target protein bands were normalized to β-actin or VDAC.

2.5. Short interfering RNA

Ovarian cancer cells were transfected using Lipofectamine RNAiMAX Reagent (#13778100, Invitrogen, Waltham, MA) and siRNA (Horizon Discovery Ltd.) targeting *MPC1*, *PYCR1*, *PYCR2*, or *PYCR3* (duplex sequences shown in Supplementary Table 1) in ABAM-free RPMI 1640 growth medium, supplemented with 10% FBS, and 2 mM glutamine. Briefly, RNAiMAX—RNAi duplex complexes were formed by adding 50 pmol of siRNA to 500 μl of reduced serum Opti-MEM (#11058021, Thermo Fisher Scientific. UK) in each well of a six-well plate, or with 50 pmol of scramble ON-TARGETplus non-targeting siRNA (#D-001810, Horizon Discovery, UK). Then, 7.5 μl RNAiMAX was added to each well containing the diluted RNAi molecules and plates were incubated at room temperature for 20 min. Exponentially growing cells were then seeded at 2×10^5 cells per well in 2.5 ml per well of ABAM-free growth media, supplemented with 10% foetal bovine serum for the indicated time in *Results*. Efficacy of mRNA depletion was assessed each time by Quantitative Real-Time (RT)-PCR or immunoblotting, for each duplex. Following 72 h siRNA treatment cells were counted using the Countess™ Automated Cell Counter (Thermo Fisher Scientific, UK) before use in further experiments.

In further experiments, cells were cultured in RPMI, DMEM or HPLM as stated in *Results*. To normalise glucose concentrations across RPMI and DMEM, high glucose DMEM media without glutamine, phenol red or sodium pyruvate (#31053044, Thermo Fisher Scientific. UK) was mixed with DMEM media without glucose, glutamine, phenol red or sodium pyruvate (#A1443001, Thermo Fisher Scientific. UK) to achieve 11.1 mM glucose growth media supplemented with ABAM. HPLM (A4899101; Thermo Fisher Scientific, UK) was supplemented with dialyzed FBS (#26400044, Thermo Fisher Scientific) and 1% ABAM.

2.6. Quantitative RT- PCR

Cells were gently washed with PBS and harvested for RNA extraction using the RNeasy Mini Kit (#74106, Qiagen, Crawley, UK.), according to the manufacturer's instructions. The purity and total RNA concentrations were determined using the NanoDrop ND-100 spectrophotometer (Labtech International, Uckfield, UK). The purity of the sample was determined at 260/280 nm and 260/230 nm range ratios, and 1 μg of total RNA added to a genomic DNA elimination reaction, followed by conversion to cDNA (#205311, QuantiTect Reverse Transcription Kit, Qiagen.), according to the manufacturer's instructions. Quantitative PCR was performed using intron-spanning primers (Supplementary Table 2) and the IQ5 system (Bio-Rad, Hemel Hempstead, UK). The arbitrary starting quantities of mRNA from experimental samples were determined using standard curves generated from serial dilutions of pooled reference RNA with QuantiFast SYBR green (#204156, Qiagen). Sample and reference genes were analysed in triplicate, and mRNA expression normalized to *ACTB* and *RPL19* (Supplementary Table 2) using the CFX Connect™ Real-time PCR detection system (Bio-Rad, UK). The PCR was performed according to SYBR green RT-qPCR protocol, using the Bio-Rad CFX Manager, version 2.1. The data was collected and analysed using CFX Connect software system. The relative expression ΔΔCq was calculated according to Livak and Schmittgen's methodology [38]. One-way ANOVA were performed on expression data normalised to *ACTB* and *RPL19*.

2.7. Stable isotope tracer analysis (SITA) by gas chromatography-mass spectrometry (GC—MS)

For sample preparation, OVCAR3 cells treated with scramble control or siRNA were cultured for 72 h and were re-seeded at 4×10^4 cells/cm^2 in a T-25 flask for the time specified in *Results*. All media used for SITA were supplemented with dialyzed FBS (A3382001; Thermo Fisher Scientific, UK). For heavy labelled glucose SITA, cells were incubated with uniformly labelled D-Glucose (U—$^{13}C_6$) (11.1 mM; #CLM-1396; CK isotopes, Leicestershire, UK) in glucose free RPMI 1640 (#11879020, Thermo Fisher Scientific) growth media for 72 h. For heavy labelled L-glutamine SITA, cells were incubated with uniformly labelled L-glutamine (U—$^{13}C_5$) (2 mM; #CLM-1822, CK isotopes, UK) in glutamine free RPMI 1640 (Thermo Fisher Scientific, #21870076) or glutamine free DMEM (Thermo Fisher Scientific, #A1443001) for 72 h. For heavy labelled L-Arginine SITA, cells were incubated for a period of 60 h and media supplemented with ^{13}C Arginine (U—$^{13}C_6$) (2 mM; #CLM-2265; CK isotopes, UK) for the final 12 h.

Following incubation with stable isotopes, cells were gently washed with ice cold saline solution and lysed in 80% methanol. Lysates were centrifuged (10,000×*g* for 10 min at 4 °C) to remove any cell debris and cell extracts were dried at 4 °C using a speed vacuum concentrator. Cellular metabolites were extracted and analysed by gas chromatography-mass spectrometry (GC—MS) using a previously described protocol [39]. Briefly, metabolite extracts were derived using N-(*tert*-butyldimethylsilyl)-N-methyl trifluoroacetamide (MTBSTFA) as described previously [40]. D-myristic acid (750 ng/sample) was added as an internal standard to metabolite extracts, and metabolite abundance was expressed relative to internal standards and normalised to cell number. GC—MS analysis was performed using an Agilent 5975C GC/MS equipped with a DB-5MS + DG (30 m × 250 μm x 0.25 μm) capillary column (Agilent J and W, Santa Clara, CA, USA). For SITA experiments, mass isotopomer distributions (MID) were determined using a custom algorithm developed at McGill University [41]. Initial matrix values for each sample were normalised to a myristic acid internal standard. Then myristic acid normalised values were normalised for cell number (MID

enrichment). Finally, all the MID enrichment values were arranged as a pint glass model to obtain total pool abundancies of ^{12}C and ^{13}C.

2.8. Clonogenic assay

An *in vitro* clonogenic assay was performed to assess the ability of a single cell to grow into a colony, following the protocol described by [42]. Briefly, cells were treated with scrambled control or targeting siRNA for 72 h. The cells were harvested and pelleted by centrifuging at 800×*g* for 5 min. Cells were resuspended in fresh RPMI media and seeded in 6-well plates at 800 cells per well in a final volume of 2.5 ml and incubated for 21 days at 37 °C in a humidified chamber containing 5% CO_2. Media was renewed on cells every 3–4 days. Following the aspiration of media from the wells, the cells were gently rinsed twice with PBS. Then, to fix and stain, 2 ml of 0.5% w/v crystal violet in 6% v/v glutaraldehyde was added to the wells. The plate was left covered in foil for 30 min at room temperature. The 0.5% w/v crystal violet in 6% v/v glutaraldehyde stain was carefully removed to avoid disturbing colonies, and the wells were rinsed by gentle submersion in water. The plates were left to dry at room temperature. The stained colonies were photographed using a Sony α7 digital camera. Colonies were manually counted by using a light microscope and the Murgaa Clicker counter (www.Murgaa.com/mac-mouse-click-counter) considering 20 cells or more as a colony.

For Haematoxylin and Eosin staining, 72 h siRNA transfected cells were detached with Accutase® (Sigma) and reseeded at 2.5×10^4 cells/ml in 2.5 ml RPMI or HPLM media in 6-well plates (7.5×10^4 cells per well) and plates incubated for a further 8 days. After incubation, cells were gently fixed with 2.5 ml of 3% paraformaldehyde for 10 min. Paraformaldehyde was removed, and 2.5 ml Haematoxylin Solution (Mayer's, Modified) (#ab220365, Abcam, UK) was added to each well and incubated for 6 min, and then washed with distilled water until water ran clear, before adding 2.5 ml Eosin Y Solution (Modified Alcoholic) (#ab246824, Abcam, UK) to each well for 2 min and washed with distilled water until water ran clear. Cells were imaged using EVOS™ XL Core Imaging System Microscope (Thermo Fisher Scientific).

2.9. *In silico* analyses

In silico analyses was undertaken using the cBioPortal for cancer genomics database at https://www.cbioportal.org [43]. The data used for analysis was a combined dataset study comprising the complete set of tumours from The Cancer Genome Atlas (TCGA) PanCancer Atlas study, profiling 32 cancer types, consisting of 10,967 samples (https://www.cancer.gov/about-nci/organization/ccg/research/structural-genomics/tcga). The data, including the mRNA expression, copy number variants (CNV), and patient survival shown in this paper were generated and pre-analysed in the original papers before being made available on cBioPortal.com. The CNV data was originally generated using the Genomic Identification of Significant Targets in Cancer (GISTIC) bioinformatic pipeline, developed by Mermel et al., from the raw sequencing data which allocates the sample a status based on the CNV: deep deletion, shallow deletion, diploid, gain, amplification [44]. The mRNA expression data was generated with RNA Seq V2 RSEM and was normalised during the Illumina sequencing process during the original data collection.

2.10. NanoString nCounter® XT gene expression assay

RNA samples were stored at −20 °C and reagents were kept at −80 °C and were thawed on ice until required. All surfaces, PCR hood, and equipment were cleaned with RNaseZAP™ (#AM9780, Thermo Fisher Scientific) to destroy any RNase. RNA concentration and quality was determined with a Nanophotometer® and samples were diluted with RNase free H_2O to 50 ng/5 μl. A master mix was created using the nCounter® XT CodeSet kit by adding 70 μl Hybridisation buffer to the Reporter CodeSet tube, mixed by inversion and spun down. Of the master mix, 8 μl was added to 5 μl of each sample in separate tubes. Then, 2 μl Capture ProbeSet was added to each sample, mixed by inversion, and spun down. Samples were incubated on a Thermo-Cycler at 65 °C for 20 h (followed by 4 °C hold).

Tubes were removed from Thermo-Cycler and spun down briefly, then made up to 35 μl with RNase free H_2O, mixed via gentle flicking, and spun down. From the samples, 13 μl were loaded to nCounter® cartridge wells, before being placed in the nCounter® SPRINT profiler System and the run initialised. The results were processed and analysed using nSolver advanced analysis software, with some graphs used directly from software output, and some raw files analysed manually.

2.11. Bioenergetic studies

The Seahorse XF^e96 analyzer (Agilent, UK) was used to measure extracellular flux upon MPC1 inhibition with UK5099, via the oxygen consumption rate (OCR; pmol/min) and the extracellular acidification rate (ECAR; mpH/min) in real-time, according to the manufacturer's instructions. Briefly, two days prior to the experiment PEO1, PEO4, or OVCAR3 cells were seeded at 3×10^4 cells per well in an XF^e96 cell culture plate, excluding several wells which were used as blanks, and cultured overnight at 37 °C in a humidified 5% CO_2 chamber. The day before the experiment cells were treated with UK5099 (5 μM) or vehicle and the cells were incubated at 37 °C and 5% CO_2 in a humidified chamber. On the day of the assay, pre-warmed Seahorse media was adjusted to pH 7.35 at 37 °C. Supernatants from the cell culture plate were gently aspirated and cells were carefully washed with 200 μl warm Seahorse RPMI media, then 150 μl of glucose- and glutamine-free Seahorse RPMI media was pipetted into each well and the plate incubated for 1 h at 37 °C in a non-CO_2 incubator. Glucose (11.1 mM) and glutamine (2 mM) solutions were diluted in Seahorse media and pH adjusted to 7.35 with sodium hydroxide (#S2770, Sigma–Aldrich). The sensor cartridge ports were loaded with 25 μl glutamine media (final concentration 2 mM) and placed in the Seahorse XF^e96 analyzer for calibration. Following the calibration, the utility plate was replaced with a cell culture plate and XF^e96 protocol was setup to measure the basal rate for 30 min then simultaneously measure OCR and ECAR for a further 2 h after injection of glucose or glutamine. Upon completion of the Seahorse XFe96 analyzer, the supernatant was carefully removed, and cells were washed gently with PBS. The cell culture plate was frozen at −80 °C for 3 h before carrying out a CyQUANT DNA quantification assay for normalisation. The data obtained were normalised to the DNA content of each well determined by the CyQUANT assay. The respiratory parameters of OCR and ECAR were calculated using the data obtained from the Seahorse XF^e96 analyzer after normalisation. Basal respiration values were normalised to the point of metabolite injection.

2.12. Enzyme-linked immunosorbent assay

Supernatants were collected from OVCAR3 cell cultures that had been targeted with siRNA or Scramble control. Human Pro-Collagen 1A1 (RRID:AB_3076400, #DY6220-05) and Human TGF-β1 (RRID:AB_2877059, #DY240-05) DuoSet® ELISA kits were purchased from R&D Systems, UK. Antibody and protein standard reagents in the kits were reconstituted as specified by the manufacturer's instructions, aliquoted and stored at −80 °C. Half-area 96 well plates (#3690, Corning, UK) were coated with capture antibody overnight at room temperature prior to conducting the assay. The TGF-β1 ELISA required

activation of supernatants prior to addition to the plate. This required the addition of 1 M HCl to 100 μl of the supernatant followed by 10 min incubation at room temperature. Then 20 μl of 1.2 M NaCl in HEPES was added to the samples. After each addition, the samples were mixed thoroughly. ELISAs were conducted as per the manufacturer's protocols. Absorbance was measured at 450 nm and 540 nm and a 4-parameter fit curve was generated to extrapolate unknown concentrations in the supernatants from known standards.

2.13. Flow cytometry

The mitochondrial superoxide ion ($O_2^{\bullet-}$) MitoSOX™ Red (#M36008, Life Technologies; ThermoFisher, UK) is oxidised by superoxide, to produce a red fluorescence (Ex/Em 510/580 nm). A 5 μM solution of MitoSOX™ Red in FACS buffer was added to 0.5 × 10^6 cells. Cells were incubated in the dark for 15 min at 37 °C with 5% CO_2, before being washed with 2 ml FACS buffer and centrifuged at 515×*g* for 7 min at 4 °C. Flow cytometry data was acquired using the ACEA NovoCyte flow cytometer and analysed using FlowJo™ (version 10.1; BD Biosciences). Appropriate controls were used including unstained and single stains to correct for fluorescence spill over. Quality control (QC) particles (Agilent, UK) were used daily to reduce inter-session instrument variability.

2.14. Statistical analysis

Raw data were handled using Microsoft Office Excel 365. The arranged data were exported to GraphPad Prism to generate graphs and statistical analyses (GraphPad Prism, version 8.3.1, USA). The Kolmogorov–Smirnoff test was used to check for normality, and data sets that deviated from normality resulted in a non-parametric test or were transformed to achieve normality. Parametric data were analysed using analysis of variance (ANOVA) for two or more groups. One-way ANOVA with either Bonferroni or Tukey's post hoc test was used to compare the treatments group with the control. For multiple comparisons, two-way ANOVA was used with Dunnett's or Šídák's multiple comparisons test. Data are presented as the mean ± standard error of the mean (SEM) unless stated otherwise. Statistics were determined from averages derived from at least three independent passages of cells unless otherwise stated. Significance values were assigned when $p \leq 0.05$ (*), $p \leq 0.05$ (**), or $p \leq 0.01$ (***).

3. RESULTS

3.1. Inhibition of MPC1 induces cell proliferation in HGSOC cell lines

As the chromosomal region encoding *MPC1* is frequently deleted or *MPC1* expression is reduced in multiple cancer types [15,17], we investigated its role in ovarian cancer. MPC1 is not detectable in ~53% of ovarian cancer cell lines [45] and strikingly, there is a copy number variant (CNV) loss of *MPC1* in nearly 80% (289 of 367) of HGSOC cases. Therefore, to investigate the role of MPC1 in ovarian cancer we used HGSOC cell lines with either low (PEO1) or relatively higher (PEO4 and OVCAR3) expression of MPC1. HEPG2 cells, which express high levels of MPC1 are shown as a comparator (Figure 1A). MPC1 and MPC2 are proposed to function as a complex [15,46,47]. Expression of the *MPC1* and *MPC2* genes differed between cells, with OVCAR3 expressing relatively high levels of *MPC1*, and PEO4 cells displaying high expression of *MPC2*, when cultured in RPMI with 2 mM glutamine (Figure 1B,C). To better represent the tumour

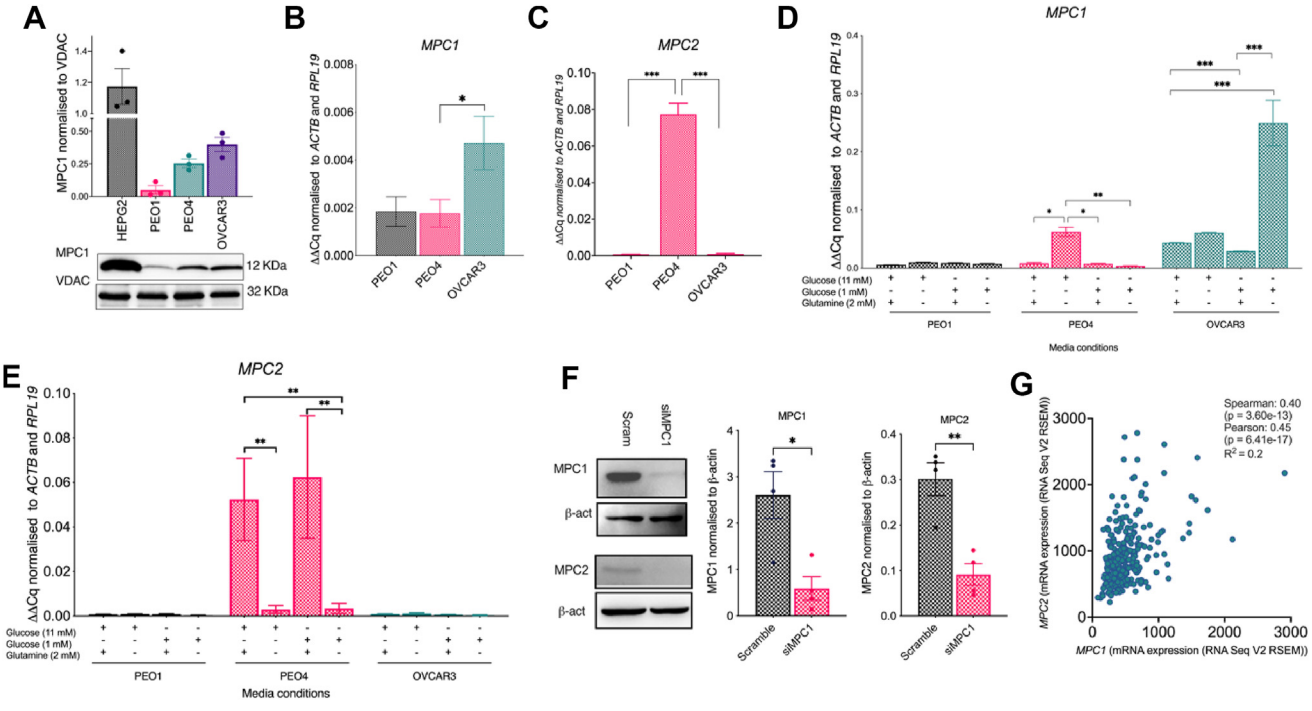

Figure 1: *MPC* expression is dependent on metabolite availability in HGSOC cells. (a) HGSOC cell lines and the HEPG2 positive control cell line were assessed for MPC1 protein expression by immunoblotting, or (b) *MPC1* or (c) *MPC2* gene expression by RT-qPCR; HGSOC cells were cultured in glucose and glutamine (11 mM, 2 mM, respectively), glucose (11 mM) without glutamine, restricted glucose (1 mM) with 2 mM glutamine or restricted glucose (1 mM) without glutamine, and expression of (d) *MPC1* or (e) *MPC2* was monitored by qPCR after 24 h; (f) OVCAR3 cells were depleted of *MPC1* by targeted siRNA for 72 h and MPC1 or MPC2 expression was assessed by immunoblotting; (g) TCGA data demonstrating correlation of *MPC1* versus *MPC2* expression in HGSOC patient tumours. Statistical significance was evaluated using an unpaired t-test or one-way ANOVA with Tukey's multiple comparison test. Data was obtained from n = 3 (A, B, C, D, E) or n = 4 (F) independent cell passages for each experiment. Data expressed as mean ± SEM (A, F) or SD (B, C, D, E); *$p \leq 0.05$, **$p \leq 0.01$ or ***$p \leq 0.001$.

microenvironment, we next determined the effect of depleting glucose or glutamine on *MPC1* or *MPC2* gene expression, under glucose (11 mM) and glutamine (2 mM) replete, glucose restricted (1 mM), or glutamine depleted (0 mM) conditions. Expression of *MPC1* was relatively low in PEO1 and PEO4 cells, except when glutamine was depleted under replete glucose conditions in PEO4 cells (Fig. 1D). OVCAR3 cells displayed relatively higher *MPC1* expression overall, which was accentuated when glutamine was depleted under restricted glucose conditions (Fig. 1D), suggesting a compensatory mechanism of *MPC1* upregulation when glucose and glutamine are restricted. MPC1 and MPC2 function as a heterodimeric complex; however, MPC2 has recently been reported to function as a homodimer transporter of pyruvate, albeit at reduced efficacy over the heterodimeric MPC complex [54], potentially explaining the lack of accumulated pyruvate in PEO4 cells, which display increased *MPC2* expression (Fig. 1C). PEO4 cells displayed increased expression of *MPC2* when glutamine (2 mM) was replete, independent of glucose concentration, which was not evident in PEO1 or OVCAR3 cells (Fig. 1E). *Whilst* low expression of MPC1 correlates with a poor prognosis in many cancer types, the effect of altered *MPC2* expression is less consistent [15]. Next, we depleted *MPC1* in OVCAR3 cells, using siRNA (Figs. S1a–c), which resulted in reduced MPC2 protein (Fig. 1F). Exploring the TCGA database, we discovered CNV gain of MPC2 in ~93% (284 of 303) of HGSOC cases. We questioned whether loss of *MPC1* also correlated with altered expression of MPC2 in patients. Accordingly, data from HGSOC patients showed a moderately positive correlation of *MPC2* with *MPC1* expression, supporting our *in vitro* data (Spearman's rank correlation coefficient = 0.4; Fig. 1G).

Using the MPC1 inhibitor UK5099, an α-cyanocinnamate analogue [48], resulted in significant increases in proliferation of PEO1 and OVCAR3 cells, represented by an increase in total cellular DNA, and an increased trend in PEO4 cells (Figs. S1d–f). Furthermore, depletion of *MPC1* increased proliferation in PEO1 cells after 72 h (Figure 2A). However, this effect was less apparent in PEO4 and OVCAR3 cells over 24 and 48 h, and at 72 h, conversely, there was a significant reduction in the number of PEO4 and OVCAR3 cells (Figure 2B,C). Next, we monitored depletion of key metabolites from the media. HGSOC cell lines treated with UK5099 metabolised approximately the same concentrations of glucose as the vehicle controls (Fig. 2E), which did not correlate with increased lactate in the cell supernatants (Fig. 2F) and we observed no substantial changes in key glycolysis pathway enzymes (Fig. S2a). Pyruvate accumulates in response to MPC inhibition in myoblasts, retinal cells, cortical neurons, and cervical cancer cells [46,49–52]. Accordingly, UK5099 treated OVCAR3 cells exhibited a significant

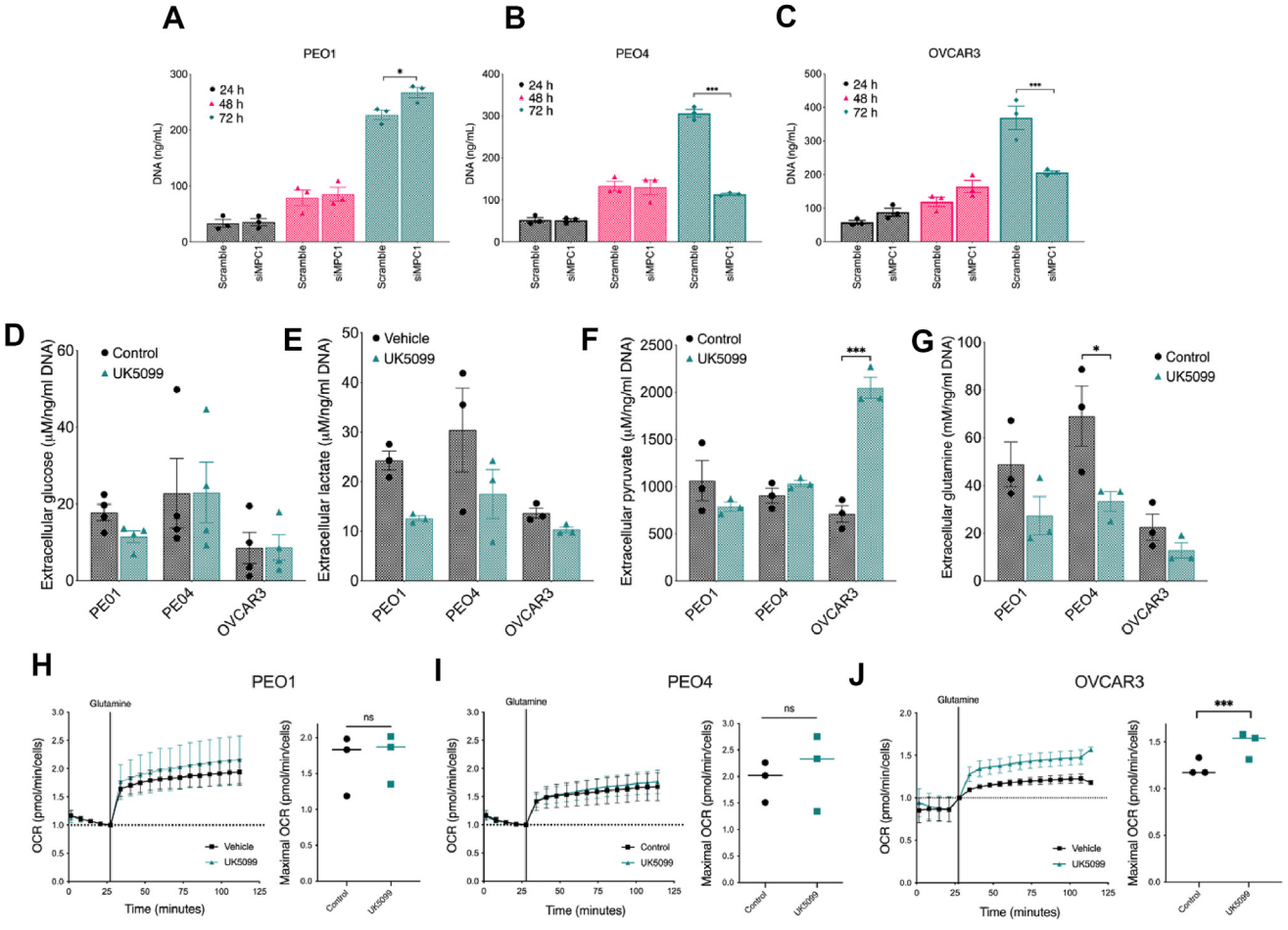

Figure 2: Depletion of *MPC1* results in accumulation of intracellular pyruvate in OVCAR3 cells and a switch to utilisation of glutamine for OXPHOS. (A) PEO1, (B) PEO4 or (C) OVCAR3 cells were depleted of *MPC1* by targeted siRNA for 72 h, cells were cultured for a further 24 h, 48 h, or 72 h, DNA concentrations were determined by lysing cells and performing the CyQUANT cell proliferation assay; HGSOC cell lines were treated with UK5099 (5 μM) for 24 h and (D) glucose, (E) lactate (F) pyruvate or (G) glutamine concentrations were assayed in cell supernatants; Oxygen consumption rate (OCR) was assayed in *MPC1* inhibited (H) PEO1, (I) PEO4 or (J) OVCAR3 cells after injection of glutamine (2 mM) in glucose-free media. Statistical significance was evaluated using one-way ANOVA with Tukey's multiple comparison test. Data was obtained from n = 3 independent cell passages for each experiment. Data expressed as mean ± SEM; *p ≤ 0.05 or ***p ≤ 0.001.

increase in extracellular pyruvate, although this was not evident in the PEO1 and PEO4 cell lines (Fig. 2G). These data suggest that pyruvate transport into the mitochondria is impaired in OVCAR3 cells upon MPC inhibition. During disrupted mitochondrial pyruvate import, glutamine oxidation has been demonstrated to maintain TCA cycling in ovarian cancer cells [53]. Therefore, we investigated whether inhibition of MPC using UK5099 would result in elevated compensatory glutamine uptake. We noted an increased trend of glutamine uptake by cells treated with UK5099, which reached significance in the PEO4 cells when compared to vehicle control (Fig. 2H). Ovarian cancers may become dependent on glutamine for tumour growth, invasion, metastasis, and resistance to chemotherapy leading to "glutamine addiction" [19–21]. Using the Seahorse XF Bioanalyzer, we explored this phenomenon further by inhibiting MPC1 with UK5099 and injecting glutamine onto HGSOC cells cultured in glucose-free media. This resulted in an increase in the oxygen consumption rate (OCR) in the HGSOC cell lines (Figure 2I–K), indicative of increased OXPHOS in response to glutamine. Furthermore, this was more apparent in the OVCAR3 cell line when MPC1 was inhibited with UK5099, compared to the vehicle control (Fig. 2K), suggesting reduced MPC function may drive ovarian cancer cells to utilise glutamine to maintain the TCA cycle. Overall, the metabolic flexibility of ovarian cancer cells may indicate a mechanism for adapting MPC complex gene expression in order to sustain ovarian cancer cell proliferation under conditions of nutrient deprivation.

3.2. Depletion of *MPC1* leads to increased abundance of nonessential amino acids

As depletion of glutamine had such an obvious effect on *MPC1* expression in OVCAR3 cells cultured in low glucose (Fig. 1D), and to avoid the confounding effects of high *MPC2* expression in PEO4 cells (Figure 1C,E), or low expression of both *MPC1* and *MPC2* in PEO1 cells, we concentrated our efforts on the OVCAR3 cell line to further study the role of MPC1 and glutamine in HGSOC cells. Moreover, given that pharmacologically, UK5099 also inhibits plasma membrane monocarboxylate transporters, albeit at K_i values two to three times higher than used here [54], and UK5099 inhibits inflammatory cytokine production independent of MPC expression [55], we further explored the role of *MPC1* in HGSOC cell proliferation and metabolism using siRNA.

Stable isotope tracer analysis (SITA) using uniformly labelled ^{13}C L-glutamine ([U−$^{13}C_5$] L-glutamine) indicated that long-term depletion of *MPC1* (Fig. S2b) resulted in an increase of the nonessential amino acid aspartate (Figure 3A), an amino acid important for the biosynthesis of nucleotide precursor purines and pyrimidines. Furthermore, tracer analysis of [U−$^{13}C_6$] D-glucose (Fig. S3c) indicated that glutamine and glucose each contributed to around half of the endogenous pool of aspartate in *MPC1* depleted OVCAR3 cells, although we found no changes in expression of the aspartate aminotransferases, *GOT1* or *GOT2* when *MPC1* was depleted (Fig. 3B). In support of our data, MPC inhibition or depletion resulted in accumulation of aspartate in mouse retina, mouse myoblasts and cortical neurons [46,49,50,52]. We also observed intracellular accumulation of the conditionally essential amino acids glycine, proline and serine (Fig. 3C). In support of this, and the observed increases in DNA in MPC1 inhibited cells (Fig. S1f), we observed increased incorporation of [U−$^{13}C_6$] D-glucose into serine and glycine when *MPC1* was depleted (Figure 3D,E). These data are consistent with previous studies in cancer, where glucose-derived carbon is shown to be diverted into *de novo* serine biosynthesis via phosphoserine aminotransferase 1 (PSAT1), potentially necessitating the generation of αKG from glutamate [56–58].

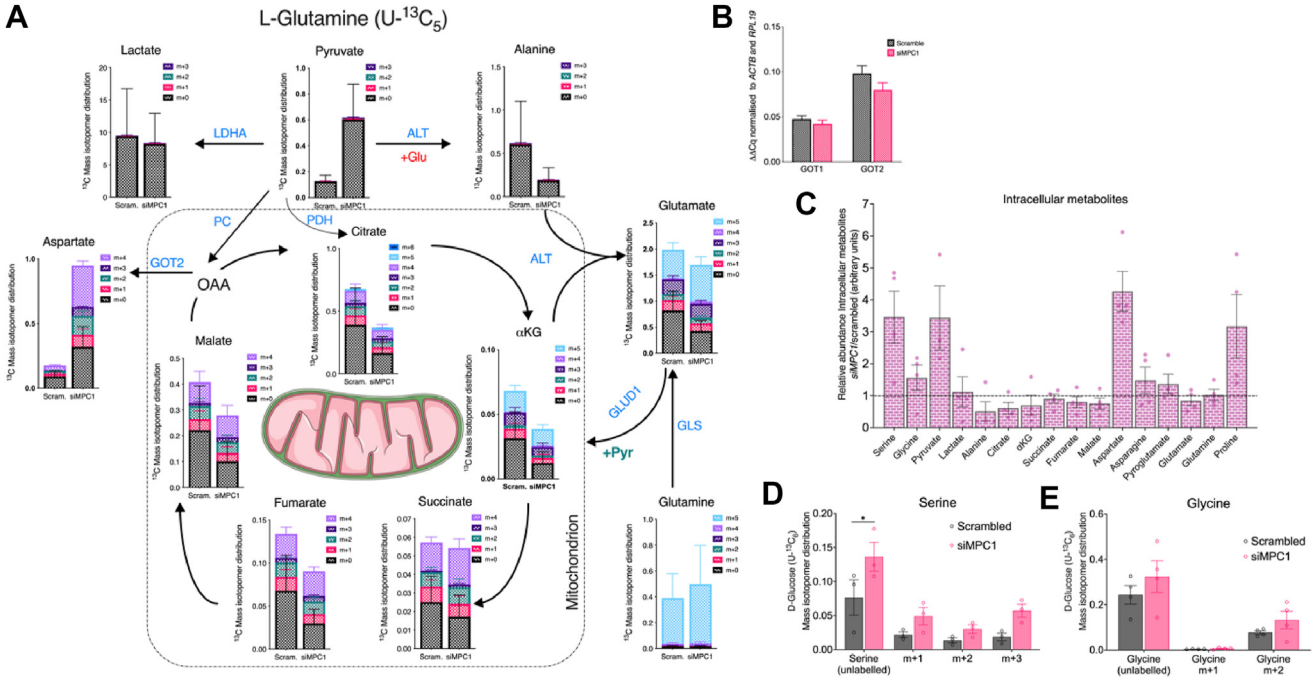

Figure 3: *MPC1* depletion influences nonessential amino acid metabolism in OVCAR3 cells. (A) mass isotopomer distribution (MID) of intracellular TCA-associated metabolites in scramble control or *MPC1* depleted OVCAR3 cells treated with L-Glutamine (U−$^{13}C_5$) for 72 h was determined by GC–MS; (B) expression of *GOT1* or *GOT2* in scramble control or *MPC1* depleted OVCAR3 cells by RT-qPCR; (C) intracellular metabolite concentrations of *MPC1* depleted cells normalised to the intracellular metabolite concentrations of the scrambled control, represented by dotted line; MID for (D) serine or (E) glycine in D-Glucose (U−$^{13}C_6$) treated OVCAR3 cells after 72 h. Statistical significance was evaluated using one-way ANOVA with Tukey's multiple comparison test. Data was obtained from n = 4 (A, C) or n = 3 (B, D, E) independent cell passages for each experiment. Data expressed as mean ± SEM; *p ≤ 0.05. Abbreviated enzyme names represent Lactate dehydrogenase A; LDHA, Alanine transaminase; ALT, pyruvate carboxylase; PC, glutaminase; GLS, glutamate dehydrogenase; GLUD1.

3.3. Depletion of *MPC1* increases cellular proline

As aforementioned, depletion of *MPC1* resulted in an increase in the conditionally essential amino acid proline (Fig. 2C). As a substrate for tumours, glutamine is considered second only to glucose [59]; however, disregarding limitations of pathway enzymes, proline and glutamine are interconvertible [22]. Thus, we reasoned that if glutamine became limited, exogenous proline may rescue cell proliferation. In agreement, cell proliferation was reduced in glutamine depleted media when MPC was inhibited and rescued by exogenous supplementation of proline (Figure 4A). Next, we further explored the role of MPC1 on OVCAR3 cell metabolism under differing culturing conditions, by comparing OVCAR3 cells cultured in [U−$^{13}C_5$] L-glutamine supplemented RPMI to cells cultured in [U−$^{13}C_5$] L-glutamine supplemented DMEM (both media contained equivalent concentrations of 10 mM glucose). Strikingly, whilst intracellular glutamine concentrations were comparable between scramble and *MPC1* depleted OVCAR3 cells cultured in [U−$^{13}C_5$] L-glutamine supplemented RPMI (Fig. 4B), in [U−$^{13}C_5$] L-glutamine supplemented DMEM the intracellular abundance of labelled glutamine was vastly reduced (by ∼93%) in *MPC1* depleted OVCAR3 cells when compared to scramble control (Fig. 4C). We hypothesised that this reduction is potentially partly due to diversion of glutamine into proline biosynthesis, as exogenous proline is not available in DMEM. To support this, we observed increased incorporation of [U−$^{13}C_5$] L-glutamine into m+5 proline in *MPC1* depleted OVCAR3 cells cultured in DMEM (Fig. 4D). Interestingly, we also noted that that there was less incorporation of labelled glutamine into aspartate in *MPC1* depleted OVCAR3 cells cultured in [U−$^{13}C_5$] L-glutamine supplemented DMEM when compared to OVCAR3 cells cultured in RPMI (Figs. S3a and S3b), whilst there was increased incorporation of labelled glutamine into pyruvate (Fig. 4E), which was not evident in [U−$^{13}C_5$] L-glutamine supplemented RPMI (Fig. 3A), indicating under certain metabolic conditions, L-glutamine can

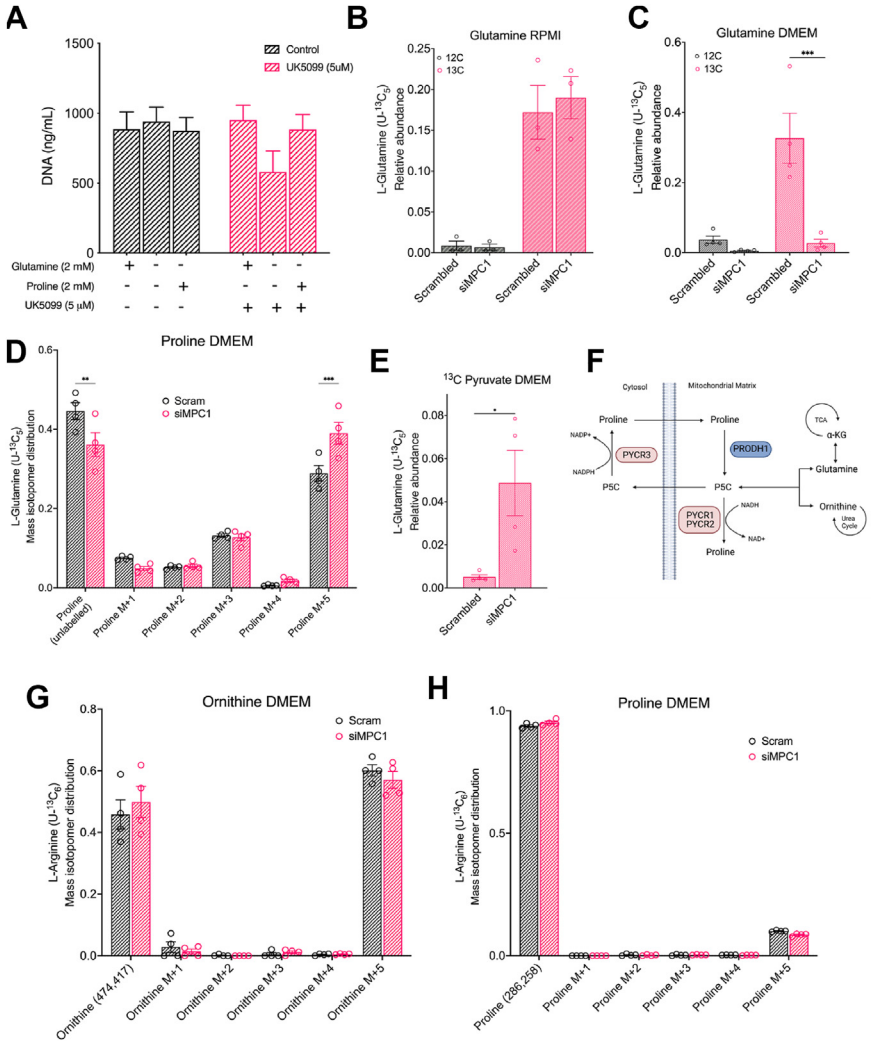

Figure 4: Media influences glutamine metabolism in *MPC1* depleted OVCAR3 cells. (A) CyQUANT analysis of proline (2 mM) supplemented OVCAR3 cells treated with UK5099 or vehicle control under glutamine replete (2 mM) or deficient (0 mM) media conditions; MID for glutamine from L-Glutamine (U−$^{13}C_5$) treated scramble control or *MPC1* depleted OVCAR3 cells cultured in (B) RPMI 1640 or (C) DMEM; MID for proline from L-Glutamine(U−$^{13}C_5$) treated scramble control or *MPC1* depleted OVCAR3 cells cultured in (D) DMEM; relative isotope abundance in pyruvate from scramble control or *MPC1* depleted OVCAR3 cells cultured in (E) DMEM; (F) a schematic of the proline biosynthetic pathway utilised from glutamate (TCA cycle) or ornithine (Urea cycle); MID for ornithine from L-Arginine (U−$^{13}C_6$) treated scramble control or *MPC1* depleted OVCAR3 cells cultured in (G) DMEM; MID for proline from L-Arginine (U−$^{13}C_6$) treated scramble control or *MPC1* depleted OVCAR3 cells cultured in (H) DMEM. Statistical significance was evaluated using one-way ANOVA with Tukey's multiple comparison test or two-way ANOVA with Šídák's multiple comparison test. Data was obtained from n = 3 (A, B) or n = 4 (C, D, E, G, H) independent cell passages for each experiment. Data expressed as mean ± SEM; **p ≤ 0.01 or ***p ≤ 0.001.

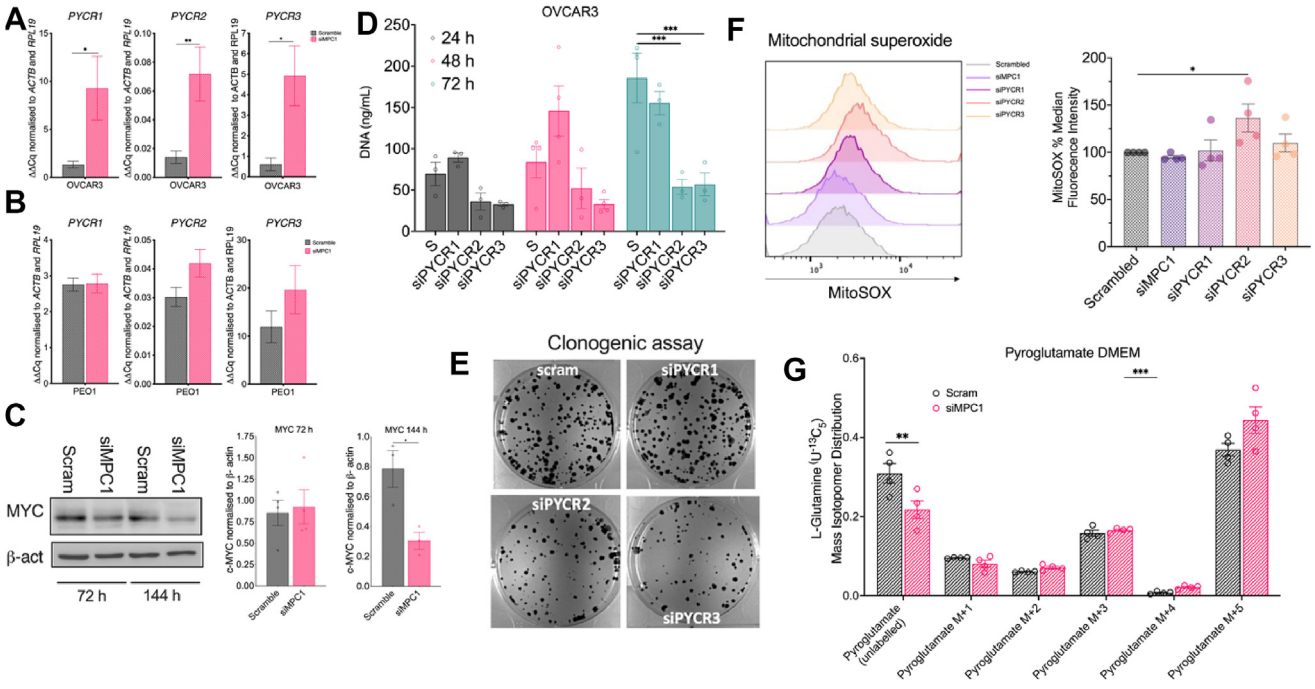

Figure 5: *PYCR2* and *PYCR3* isozymes are critical for HGSOC proliferation and colony formation: (A) OVCAR3 or (B) PEO1 expression of *PYCR1, PYCR2* or *PYCR3* by qPCR in scramble control or *MPC1* depleted cells over 24 h; (C) MYC protein abundance in scramble control or *MPC1* depleted OVCAR3 cells after 72 h or 144 h siRNA; (D) CyQUANT cell proliferation assay assessing the DNA concentration of OVCAR3 cells at 24 h, 48 h or 72 h under *PYCR1, PYCR2* or *PYCR3* depleted conditions; (E) clonogenic assay of OVCAR3 cells cultured for 21 days following *PYCR1, PYCR2* or *PYCR3* depletion; (F) MitoSOX™ assay measuring the mitochondrial ROS produced by *MPC1*, *PYCR1*, *PYCR2* or *PYCR3* depleted cells; (G) MID for pyroglutamate from L-Glutamine (U−$^{13}C_5$) treated scramble control or *MPC1* depleted OVCAR3 cells cultured in DMEM. Statistical significance was evaluated using a unpaired t-test or one-way ANOVA with Tukey's multiple comparison test or two-way ANOVA with Šídák's multiple comparison test. Data was obtained from n = 2 (E), n = 3 (A, B) or n = 4 (C, D, F, G) independent biological cell passages for each experiment. Data expressed as mean ± SD (A, B) or SEM (C, D, F, G); *p ≤ 0.05, **p ≤ 0.01 or ***p ≤ 0.001.

contribute to pyruvate when mitochondrial pyruvate transport is impaired.

Mitochondrial PYCR1 and PYCR2 isozymes are essential for colorectal cancer cell proliferation and survival [60]. Initially, Δ^1-pyrroline-5-carboxylate synthetase (P5CS/ALDH18A1) converts glutamate to Δ^1-pyrroline-5-carboxylate (P5C), followed by the conversion of P5C to proline via mitochondrial PYCR1 or mitochondrial/cytosolic PYCR2. Alternatively, ornithine derived P5C can be metabolised to proline via a cytosolic PYCR3 isozyme (also known as PYCRL; Fig. 4F) [22,61]. The cytosolic PYCR3 isozyme utilises ornithine, an arginine-derived intermediate, rather than glutamate [62]. Defective arginine synthesis, known as arginine auxotrophy, is a common metabolic vulnerability in cancer and the rate-limiting enzyme for arginine synthesis, argininosuccinate synthetase (ASS1), is expressed at high levels in primary HGSOC cases [63] and in OVCAR3 cells [64]. Here, in OVCAR3 cells, treated with [U−$^{13}C_6$] L-arginine for 12 h, L-arginine contributed >50% of the intracellular pool of ornithine (M+5; Fig. 4G), with a smaller proportion contributing to proline (M+5), although there were no observed significant differences in cells depleted of *MPC1* (Fig. 4H). Overall, these data indicate that ovarian cancer cells adapt to exogenous amino acid availabilities to maintain *de novo* proline biosynthesis.

3.4. PYCR isozymes play a role in proliferation and redox homeostasis

Next, we assessed expression of the key isozymes involved in the *de novo* biosynthesis of proline to determine whether any changes are driven my MPC1 loss/inhibition. Consistent with our hypothesis, depletion of *MPC1* resulted in OVCAR3 cells significantly increasing expression of PYCR isozyme genes (Figure 5A), which was not evident in the relatively low *MPC1/MPC2* expressing PEO1 ovarian cancer cells (Figure 1A,B and 4b). According to TCGA, *MYC* is overexpressed in >50% of HGSOC cases. Previous studies have shown that altered proline metabolism and increased PYCR expression in cancer are driven by MYC [65,66]. In support of TCGA data, we observed high expression of MYC in scramble control cells, which did not significantly alter with *MPC1* depletion. However, after 144 h *MPC1* depletion MYC abundance was shown to be reduced (Fig. 5C). To further explore a role for PYCR isozymes in ovarian cancer cell proliferation and colony formation, we depleted *PYCR1*, *PYCR2*, or *PYCR3* (Figs. S4a–c) in OVCAR3 cells for 72 h and reseeded for 24 h, 48 h, 72 h or for 21 days in a colony formation assay. Here, the PYCR2 and PYCR3 isozymes, but not PYCR1, were critical for cell proliferation (Fig. 5D) and colony formation in OVCAR3 cells (Fig. 5E). Proline dehydrogenase (PRODH) and PYCRs form a metabolic relationship known as the proline−P5C cycle. The catabolism of proline is mediated by PRODH, in the reverse reaction to that catalysed by PYCR isozymes from P5C. The proline-P5C cycle mediated by PRODH and PYCR isozymes link mitochondria and the cytosol to maintain redox homeostasis [67,68]. Furthermore, proline biosynthesis functions as a vent for TGF-β induced mitochondrial redox stress in cancer associated fibroblasts [69]. We therefore next assessed mitochondrial ROS, using the mitochondrial superoxide probe, MitoSOX. Depletion of *PYCR2*, but not *PYCR1* or *PYCR3* isozymes, resulted in a ∼35% increase in MitoSOX (Fig. 5F). Kuo et al. demonstrated PYCR2 protects cells from overt stress by interacting with RRMB2 [70]. Using SITA, we also noted significantly increased incorporation of [U−$^{13}C_5$] L-glutamine into pyroglutamate (M+5; Fig. 5F) in *MPC1* depleted cells. Altered pyroglutamate is indicative of a decrease in ATP or a turnover of glutathione in cells, due

to increased oxidative stress [71,72]. Taken together, these results demonstrate that MPC1 and PYCR isozymes play a role in HGSOC cell proliferation and suppression of oxidative stress.

3.5. MPC1 and PYCR isozymes orchestrate HGSOC collagen production

Collagen remodelling genes, regulated by TGF-β signalling, promote metastasis of ovarian cancer cells and correlate with a poor overall survival in serous ovarian cancer patients [73]. As proline metabolism is particularly important for the production of collagen, we next investigated whether the PYCR isozymes play a role in ovarian cancer cell TGF-β production by depleting *MPC1* or PYCR isozymes to assess their effect on TGF-β production. Whilst depletion of *MPC1* did not alter TGF-β, depletion of PYCRs resulted in reduced extracellular TGF-β (Figure 6A). As TGF-β production was affected by depletion of PYCR isozymes, we next looked at their role in the expression of collagen proteins. Collagen type I alpha 1 chain (*COL1A1*) expression is correlated with resistance of ovarian cancer to cisplatin and Taxol [74,75]. We observed Pro-COL1A1 to be increased in cell supernatants when *PYCR2* or *PYCR3* was depleted (Fig. 6B). Type VI collagen expression correlates with grade of ovarian tumour, metastasis, resistance to cisplatin and worse patient overall survival [34,73,76]. Immunoblotting demonstrated Type VI collagen was not basally expressed in OVCAR3 cells, however, when *MPC1* and *PYCR2* were co-depleted in these cells, there was a robust increase in Type VI collagen protein abundance (Fig. 6C). Overall, these data suggest MPC1 and PYCR isozymes work in concert to regulate collagen production in HGSOC cells.

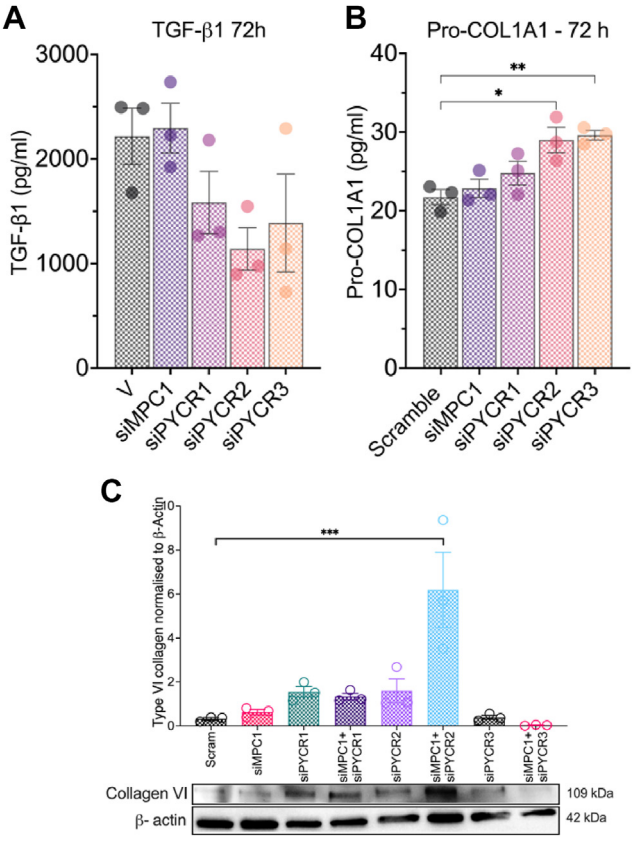

Figure 6: PYCR isozymes orchestrate TFG-β1 and collagen production in OVCAR3 cells. (A) TGF-β1 production in supernatants from Scrambled control treated, or *MPC1*, *PYCR1*, *PYCR2*, or *PYCR3* depleted OVCAR3 cells after 72 h; (B) Pro-COL1A1 production in supernatants from Scrambled control treated, or *MPC1*, *PYCR1*, *PYCR2*, or *PYCR3* depleted OVCAR3 cells after 72 h; (C) immunoblotting for Collagen VI production in Scrambled control treated, or *MPC1*, *PYCR1*, *PYCR2*, or *PYCR3* depleted OVCAR3 cells alone or in combination after 72 h. Statistical significance was evaluated using one-way ANOVA with Tukey's multiple comparison test or two-way ANOVA with Šídák's multiple comparison test. Data was obtained from n = 3 independent biological cell passages for each experiment. Data expressed as mean ± SEM; *p ≤ 0.05, **p ≤ 0.01 or ***p ≤ 0.001.

3.6. PYCR isozymes are overexpressed in HGSOC patients

As depletion of *PYCR2* or *PYCR3* had similar effects on reducing OVCAR3 cell viability (Fig. 4B) and colony formation (Fig. 4D), we next explored TCGA to assess their expression in HGSOC patients. The expression of PYCR2 has previously been demonstrated to be ∼5.8 times higher in chemotherapy resistant versus chemotherapy naïve ascites derived tumour cells [77]. In HGSOC patients, the *PYCR1* or *PYCR2* genes were over expressed in around 3% and ∼14% of cases, respectively, with copy number gain of *PYCR2* in 75% of cases (114/152 HGSOC patients). Patients also displayed copy number gain of *PCYR3* in 92% of cases, with 1 in 3 patients displaying mRNA amplification of *PYCR3* (102 of 311 cases) and 44% of cases reporting high mRNA (Figure 7A). Furthermore, across 33 different types of cancers profiled in TCGA (10,945 patients), *PYCR3* was amplified the most in HGSOC patients (Fig. 7B) and increased expression of *PYCR3* equated to an ovarian cancer diagnosis at an earlier age of 54-years compared to 63-years (Fig. 7C). Furthermore, increased expression of *PYCR3* was associated with more aggressive disease indicated clinically by significantly increased vascular invasion (TCGA). Taken together, these data suggest that amplification of *PYCR3* correlates with more aggressive disease *in vitro* and *in vivo* and represents a promising novel target in the treatment of HGSOC. To further explore the roles of PYCR isozymes in HGSOC cells, we used the physiologically representative Human Plasma-Like Medium (HPLM). In support of the previous clonogenic assay data over 21 days (Fig. 5E), OVCAR3 cell proliferation was reduced by depletion of *PYCR2* or *PYCR3,* which was further exacerbated by culturing cells in physiologically relevant HPLM versus RPMI media (Fig. 7D).

As *PYCR3* is overexpressed in approximately a third of HGSOC patients, we focused on targeting PYCR3. Therefore, we next depleted *PYCR3* in OVCAR3 cells cultured in HPLM and assayed changes in metabolic gene expression using a NanoString nCounter Metabolic Pathways Panel. We showed increased tumour necrosis factor (*TNF*) (Fig. 7F) and lymphotoxin-beta (*LTB*) in *PYCR3* depleted cells (Fig. 7G). The TNF superfamily (TNFSF) member 14 (TNFSF14) LIGHT, which has a role in antitumour immunity, interacts with diverse cells within the tumour microenvironment via lymphotoxin β receptor (LTβR) [78]. Furthermore, folate receptor alpha (*FOLR1*) expression was reduced in *PYCR3* depleted OVCAR3 cells (Fig. 7H). The *FOLR1* gene has been reported to be highly overexpressed in ovarian cancer, driving ovarian tumour proliferation and invasion [79] and is associated with cisplatin treatment resistance [80]. Overall, this data indicates that targeting *PYCR3* could potentiate antitumour immunity and reduce tumour proliferation and invasion (Figure 8).

4. DISCUSSION

Tumour-associated genetic alterations result in dysregulation of cancer cell metabolic pathways, facilitating nutrient acquisition in a typically nutrient-restricted tumour microenvironment [27,81]. The reduced expression of *MPC1* or *MPC2*, key orchestrators of pyruvate import into the mitochondrial matrix [82], correlates with poor prognoses in several cancer types including head and neck, lung, colon, kidney, and prostate [15,16,83–86]. As data from TCGA indicates that the chromosomal

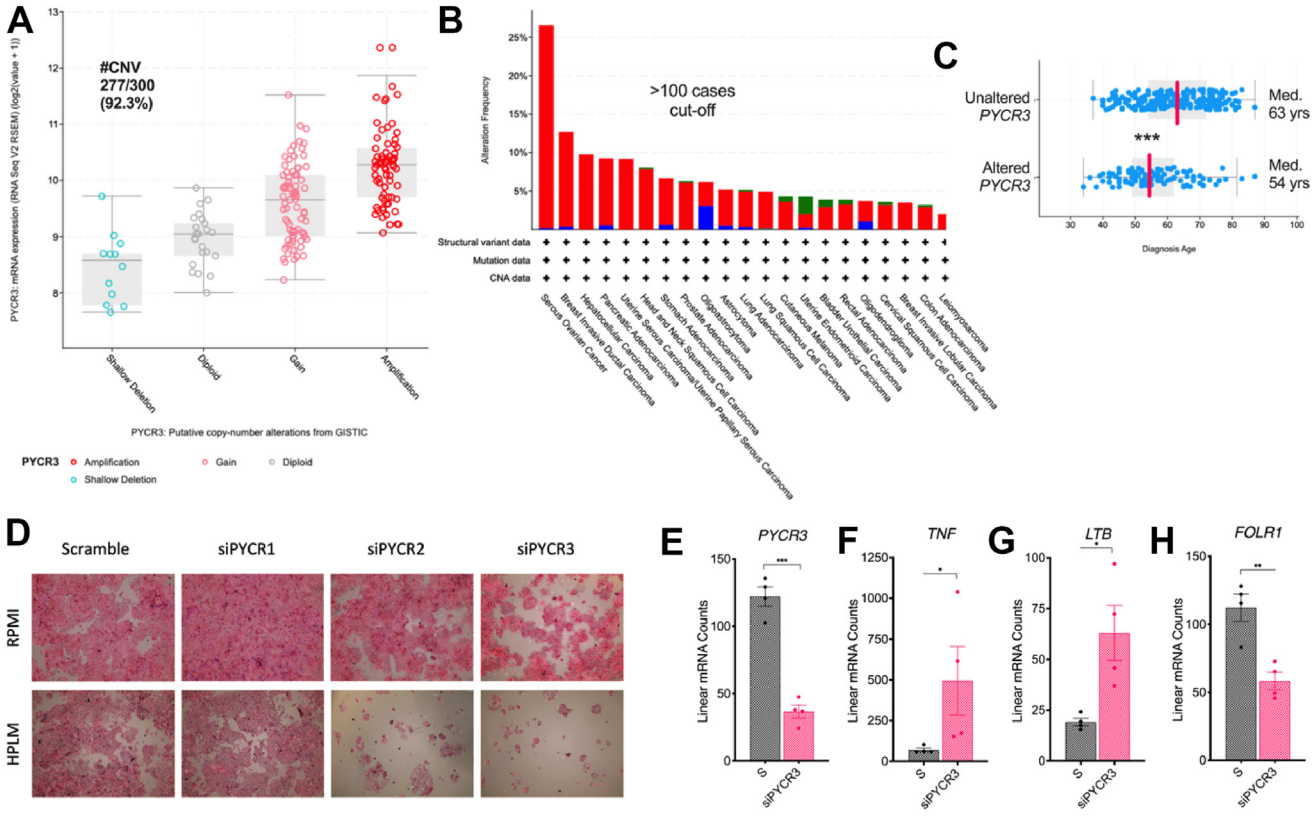

Figure 7: More than one third of HGSOC patients display increased *PYCR3* expression, depletion of *PYCR3* reduces colony formation. (A) TCGA data demonstrates 92.3% copy number variance of the *PYCR3* gene, and increased *PYCR3* mRNA expression vs putative copy-number of *PYCR3*, in 300 HGSOC patient tumours compared to normal tissue (shallow deletion, blue; diploid, grey; gain, light-red; and amplification, red); (B) alteration frequency of *PYCR3* across all cancers profiled by TCGA with >100 cases per cancer (red, amplification); (C) Median diagnosis age in unaltered or altered *PYCR3* HGSOC cases; (D) targeting of *PYCR1, PYCR2, or PYCR3* in OVCAR3 cells cultured in RPMI or HPLM media for 8 days and stained with eosin; (E) NanoString analysis of *PYCR3* depletion in OVCAR3 cells: expression of (F) *TNF,* (G) *LTB,* or (H) *FOLR1*. Statistical significance was evaluated using one-way ANOVA with Tukey's multiple comparison or unpaired t-test. Data was obtained from n = 3 or n = 4 independent cell passages for each experiment. Data expressed as mean ± SEM; *p ≤ 0.05, **p ≤ 0.01 or ***p ≤ 0.001. (For interpretation of the references to color/colour in this figure legend, the reader is referred to the Web version of this article.)

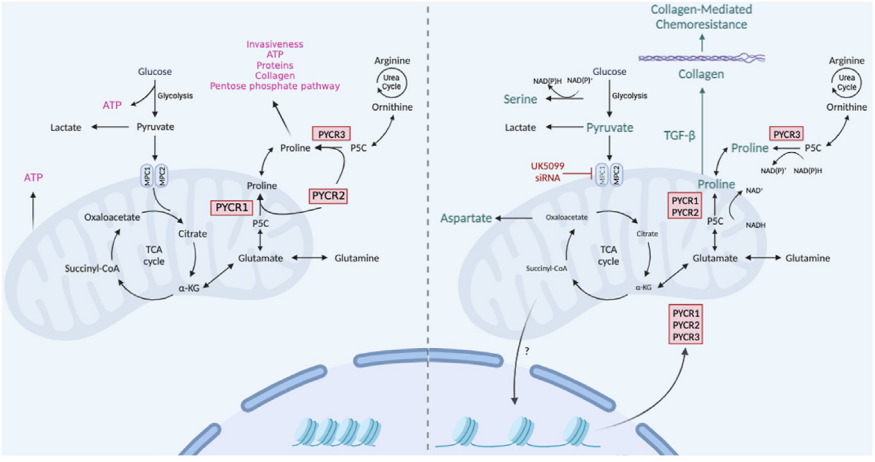

Figure 8: Loss of MPC1 alters proline metabolism and collagen production. MPC1: Mitochondrial Pyruvate Carrier 1; MPC2: Mitochondrial Pyruvate Carrier 2; PYCR: pyrroline-5-carboxylate reductase; P5C: 1-Pyrroline-5-carboxylic acid; ATP: Adenosine triphosphate; α-KG: alpha-ketoglutarate; NAD(P)H: Reduced nicotinamide adenine dinucleotide (phosphate); NAD(P): Nicotinamide adenine dinucleotide (phosphate).

locus for *MPC1* shows CNV loss in >80% ovarian cancer patient cases [15,17], our aim was to investigate the role of MPC1 in ovarian cancer progression. Our data indicates short-term inhibition of *MPC1* in ovarian cancer cells results in increased cell proliferation, whilst chronic depletion of *MPC1* results in increased expression of PYCR isozymes, key enzymes involved in the final step of proline biosynthesis. We show that HGSOC colony formation is dependent on *PYCR2* and *PYCR3,* a gene found to be most overexpressed in ovarian cancer, compared to all other tumour types profiled (>10,000 cases) on the TCGA database. We also demonstrated that PYCRs are required for ovarian cancer cell TGF-β1 production, a known driver of both fibrosis and malignancy, and that *MPC1* and PYCR isozymes orchestrate the production of collagen proteins known to be important in ovarian cancer progression and resistance to chemo- and immunotherapies (Fig. 8) [33,34].

Loss of MPC function mimics a glucose depleted tumour microenvironment, initiating compensatory cellular metabolism, including glutamine anaplerosis [46]. Previous work has established a key role for glutamine in maintaining the TCA cycle upon inhibition of MPC1 [18]. Here, we show depletion of *MPC1* resulted in glutamine-dependent increases in proliferation of ovarian cancer cell lines in the short-term and considerable pyruvate accumulation in high MPC1 expressing ovarian cancer cells. MPC1 and MPC2 are proposed to function as a complex [15,46,47] and more recent evidence suggests MPC2 can function independently of MPC1 [87]. Interestingly, OVCAR3 cells with low *MPC2* expression accumulated pyruvate which was not evident in the high MPC2 expressing PEO4 cells, suggesting MPC2 may compensate for loss of MPC1 and maintain mitochondrial pyruvate influx in these cells.

Metabolic studies using engineered biosensors or ^{13}C-enriched substrates to monitor pyruvate metabolism have shown reduced activity of MPC-dependent metabolic pathways in cancers [18,88]. Circulating concentrations of aspartate are amongst the lowest of all the circulating amino acids. Aspartate synthesis is dependent on the electron transport chain and is an endogenous metabolic limitation in cancer cell proliferation and tumour growth [89–91]. Here, in metabolic tracing studies we show depletion of *MPC1* resulted in a 6-fold increase in endogenous aspartate and decreased alanine abundance, with the majority of enriched aspartate derived from ^{13}C-glutamine via the TCA cycle. Furthermore, our results demonstrated no change in expression of aspartate aminotransferases in *MPC1* depleted ovarian cancer cells, in contrast to other studies showing increased aspartate dependence on oxaloacetate and GOT2 [50]. Furthermore, whilst still significant, the observed increase in aspartate in *MPC1* depleted cells, when compared to scramble control, was reduced when cultured in DMEM rather than RPMI. In support of our data, previous studies have reported increased aspartate and reduced alanine abundances in mouse retina, mouse myoblasts and cortical neurons [46,49,50,52], although in some cases this was in response to depletion of *Mpc2*, not *Mpc1* [46]. Despite several studies reporting this phenomenon, the cell signalling processes controlling the fate of aspartate upon MPC depletion remain unclear and require further exploration.

Inhibition of MPC1 induced OVCAR3 cancer cells to switch to glutamine for OXPHOS, which was not evident in PEO4 cells, although as aforementioned, the necessity to utilise glutamine may be reduced in these cells due to increased expression and utilisation of MPC2 [87]. We also noted increased intracellular proline upon prolonged depletion of *MPC1* in OVCAR3 cells. Interestingly, Schell et al. showed a selective pressure against high MPC1 expression in cancer cells grown in anchorage-free conditions *in vitro* or *in vivo* [92] and, in a recent study, Pilley et al. reported that proline accumulated to high levels in a 3D cultured, rather than 2D cultured, colorectal cancer cell line (HCT116). Moreover, proline did not begin to accumulate until at least 24 h after detachment of the cells [31]. PYCR isozymes, involved in proline biosynthesis from glutamine or ornithine, are upregulated in various cancer types with *PYCR1* reported to be the most overexpressed metabolic enzyme overall, driving metastasis and tumour growth [62]. We demonstrated depletion of *MPC1* resulted in upregulation of *PYCR1*, *PYCR2* and *PYCR3* genes. Although, from SITA, neither ^{13}C-enriched glucose or glutamine were initially traced through to the increased intracellular proline observed in *MPC1* depleted ovarian cancer cells. However, as RPMI 1640 media is supplemented with proline (0.17 mM), we also used unsupplemented DMEM. Cells that were depleted of *MPC1* and cultured in DMEM displayed exhaustion of most of their intracellular glutamine over 72 h and displayed increased ^{13}C-labelled (m+5) proline, that was also evident in the control cells, suggesting loss of exogenous proline (or other metabolites present in RPMI) could result in diversion of glutamine into proline biosynthesis. Unlabelled proline could also be derived from arginine via PYCR3. Therefore, we cultured *MPC1* depleted cells with ^{13}C-arginine enriched DMEM and traced a significant proportion of arginine through to ornithine and to a lesser extent proline. Although, this could be due to the cells only being exposed to labelled arginine for 12 h. Therefore, under some circumstances the cytosolic PYCR3 isozyme, that reportedly exclusively utilises ornithine rather than glutamine for proline synthesis, may play an important role in proline biosynthesis in ovarian cancer cells [62].

Depletion of *MPC1* may result in a pseudohypoxic state (reduced flux of pyruvate into mitochondria) for cancer cells, due to reduced electron transport chain activity, supported by reduced basal OCR in UK5099 inhibited ovarian cancer cells. The PYCR1 isozyme supports proliferation under oxygen-limiting conditions [93], and proline biosynthesis from glutamine in *IDH1* mutant cells, permitting the TCA cycle to progress *in lieu* of oxygen consumption [94], potentially explaining the exhaustion of intracellular glutamine upon depletion of *MPC1*, observed here. Depletion of *PYCR1* did not reduce colony formation in ovarian cancer cells; however, depletion of *PYCR2* (mitochondrial glutamine/cytosolic ornithine) or *PYCR3* (cytosolic ornithine) resulted in reduced OVCAR3 cell proliferation and colony formation, particularly when cells were cultured in the more physiologically representative HPLM. Furthermore, depletion of *PYCR3* altered key genes involved in ovarian cancer progression and therapy-sensitivity, including reduced expression of *FOLR1*, which is expressed in the majority of ovarian carcinomas, including in up to 76% of HGSOC cases [95].

Although less explored than PYCR1, previous studies employing metabolomic profiling identify PYCR2 as the most significantly altered protein involved in amino acid metabolism in hepatocellular and oesophageal squamous cell carcinomas [96,97]. Tumours with relatively high PYCR2 also display upregulation of pathways involved in DNA replication [98]. As for PYCR1, increased expression of *PYCR2* may also permit cells to cope with excessive oxidative species as a consequence of increased metabolic activity, as loss of PYCR2 is demonstrated to result in apoptosis from oxidative stress [99]. Here, loss of *PYCR2* resulted in a ~35% increase in superoxide production ($O2^{\bullet-}$) in OVCAR3 cells, suggesting PYCR2 is involved in controlling oxidative stress in these cells.

The desmoplastic subtype of HGSOC represents the poorest prognosis, highlighting the contribution of the ECM in ovarian cancer progression [100,101]. Adhesion of cancer cells to ECM enhances tumorigenicity and confers resistance to chemotherapeutic agents [102]. As PYCR are important in collagen biosynthesis and COL6A3 has previously been demonstrated to be important in ovarian cancer progression, we investigated whether *MPC1* depletion and PYCR gene expression played a role in collagen formation. Remarkably, depletion of *PYCR2* in

conjunction with MPC1 resulted in increased expression of collagen VI in the OVCAR3 cell line. As aforementioned, depletion of *MPC1* favours anchorage-independent growth [92]; previous studies show cancer cells grown in 3D show increased expression of collagen VI [31]. The C5 subdomain of collagen Type VI α3 is immediately cleaved off after secretion, known as endotrophin, a molecule with potent pro-tumorigenic signalling capacity in breast and colon cancers [103–105]. Endotrophin induces pulmonary breast cancer metastasis by inducing TGF-β dependent epithelial mesenchymal transition i*n vivo* [105]. Type VI collagen is also a biomarker for pancreatic cancer and is elevated in the serum of breast cancer patients [106,107], so these findings may be important for tumour progression in other cancer types. Although, the key events that orchestrate this switch from proliferation to collagen Type VI biosynthesis remain to be determined. Here, we provide a mechanistic understanding underlying the role of *MPC1* in ovarian cancer. Although, it must be noted that the three representative HGSOC cell lines used in this study displayed diverse *MPC1* and *MPC2* expression, which was further influenced by the presence of glutamine in the media. However, overall we show MPC1 is involved in dysregulated pyruvate metabolism, the metabolic reprogramming of PYCR expression and proline biosynthesis, redox balance, and collagen formation, all of which may play an important role in ovarian cancer progression and therapy resistance.

CREDIT AUTHORSHIP CONTRIBUTION STATEMENT

M.R. Farook: Conceptualization, Data curation, Formal analysis, Methodology, Writing — original draft, Writing — review & editing. **Z. Croxford:** Data curation, Formal analysis, Methodology. **S. Morgan:** Data curation. **A.D. Horlock:** Data curation, Methodology, Writing — review & editing. **A. Holt:** Data curation, Formal analysis. **A. Rees:** Data curation, Formal analysis. **B.J. Jenkins:** Data curation, Formal analysis. **C. Tse:** Data curation. **E. Stanton:** Data curation. **D.M. Davies:** Conceptualization. **C.A. Thornton:** Conceptualization. **N. Jones:** Conceptualization, Data curation, Formal analysis, Investigation, Methodology, Writing — original draft, Writing — review & editing. **I.M. Sheldon:** Conceptualization, Writing — review & editing, Supervision. **E.E. Vincent:** Conceptualization, Data curation, Formal analysis, Writing — original draft, Writing — review & editing. **J.G. Cronin:** Conceptualization, Data curation, Formal analysis, Funding acquisition, Investigation, Methodology, Project administration, Resources, Supervision, Writing — original draft, Writing — review & editing.

ACKNOWLEDGEMENTS

This work here was in part supported by grants awarded by St David's Medical Foundation, Registered Charity No. 1122688; the Welsh Government in support of the C81844/C81845 ACCELERATE (Welsh Health Innovation Technology Accelerator) project. The results published here are part based upon data generated by The Cancer Genome Atlas (TCGA) Research Network: https://www.cancer.gov/tcga. EEV was supported by Cancer Research UK [grant number C18281/A29019]. NJ was supported by a New Investigator Research Grant from the Medical Research Council, United Kingdom [grant number MR/X000095/1].

DECLARATION OF COMPETING INTEREST

The authors declare that they have no known competing financial interests or personal relationships that could have appeared to influence the work reported in this paper.

DATA AVAILABILITY

No data was used for the research described in the article.

APPENDIX A. SUPPLEMENTARY DATA

Supplementary data to this article can be found online at https://doi.org/10.1016/j.molmet.2024.101900.

REFERENCES

[1] Reid BM, Permuth JB, Sellers TA. Epidemiology of ovarian cancer: a review. Cancer Biology & Medicine 2017;14(1):9–32.
[2] Lisio MA, Fu LL, Goyeneche A, Gao ZH, Telleria C. High-grade serous ovarian cancer: basic sciences, clinical and therapeutic standpoints. Int J Mol Sci 2019;20(4).
[3] Langyel E. Ovarian cancer development and metastasis. Am J Pathol 2010;177(3):1053–64.
[4] Nieman KM, Kenny HA, Penicka CV, Ladanyi A, Buell-Gutbrod R, Zillhardt MR, et al. Adipocytes promote ovarian cancer metastasis and provide energy for rapid tumor growth. Nat Med 2011;17(11). 1498-U1207.
[5] Matulonis UA, Sood AK, Fallowfield L, Howitt BE, Sehouli J, Karlan BY. Ovarian cancer. Nat Rev Dis Prim 2016;2:22.
[6] Lieu EL, Nguyen T, Rhyne S, Kim J. Amino acids in cancer. Exp Mol Med 2020;52(1):15–30.
[7] Desbats MA, Giacomini I, Prayer-Galetti T, Montopoli M. Metabolic plasticity in chemotherapy resistance. Front Oncol 2020;10.
[8] Ahmed N, Escalona R, Leung D, Chan E, Kannourakis G. Tumour microenvironment and metabolic plasticity in cancer and cancer stem cells: perspectives on metabolic and immune regulatory signatures in chemoresistant ovarian cancer stem cells. Semin Cancer Biol 2018;53:265–81.
[9] Yang L, Moss T, Mangala LS, Marini J, Zhao H, Wahlig S, et al. Metabolic shifts toward glutamine regulate tumor growth, invasion and bioenergetics in ovarian cancer. Mol Syst Biol 2014;10(5):728.
[10] Yang LF, Moss T, Mangala LS, Marini J, Zhao HY, Wahlig S, et al. Metabolic shifts toward glutamine regulate tumor growth, invasion and bioenergetics in ovarian cancer. Mol Syst Biol 2014;10(5):23.
[11] Wang X, Zhao X, Zhao J, Yang T, Zhang F, Liu L. Serum metabolite signatures of epithelial ovarian cancer based on targeted metabolomics. Clin Chim Acta 2021;518:59–69.
[12] Liberti MV, Locasale JW. The warburg effect: how does it benefit cancer cells? Trends Biochem Sci 2016;41(3):211–8.
[13] DeBerardinis RJ, Mancuso A, Daikhin E, Nissim I, Yudkoff M, Wehrli S, et al. Beyond aerobic glycolysis: transformed cells can engage in glutamine metabolism that exceeds the requirement for protein and nucleotide synthesis. Proc Natl Acad Sci U S A 2007;104(49):19345–50.
[14] Herzig S, Raemy E, Montessuit S, Veuthey JL, Zamboni N, Westermann B, et al. Identification and functional expression of the mitochondrial pyruvate carrier. Science 2012;337(6090):93–6.
[15] Schell JC, Olson KA, Jiang L, Hawkins AJ, Van Vranken JG, Xie J, et al. A role for the mitochondrial pyruvate carrier as a repressor of the Warburg effect and colon cancer cell growth. Mol Cell 2014;56(3):400–13.
[16] Bensard CL, Wisidagama DR, Olson KA, Berg JA, Krah NM, Schell JC, et al. Regulation of tumor initiation by the mitochondrial pyruvate carrier. Cell Metabol 2020;31(2):284–300 e287.
[17] Tibiletti MG, Trubia M, Ponti E, Sessa L, Acquati F, Furlan D, et al. Physical map of the D6S149-D6S193 region on chromosome 6q27 and its involvement in benign surface epithelial ovarian tumours. Oncogene 1998;16(12):1639–42.

[18] Yang C, Ko B, Hensley CT, Jiang L, Wasti AT, Kim J, et al. Glutamine oxidation maintains the TCA cycle and cell survival during impaired mitochondrial pyruvate transport. Mol Cell 2014;56(3):414–24.

[19] Yang L, Moss T, Mangala LS, Marini J, Zhao H, Wahlig S, et al. Metabolic shifts toward glutamine regulate tumor growth, invasion and bioenergetics in ovarian cancer. Mol Syst Biol 2014;10:728.

[20] Masamha CP, LaFontaine P. Molecular targeting of glutaminase sensitizes ovarian cancer cells to chemotherapy. J Cell Biochem 2018;119(7):6136–45.

[21] Wise DR, Thompson CB. Glutamine addiction: a new therapeutic target in cancer. Trends Biochem Sci 2010;35(8):427–33.

[22] Phang JM, Liu W, Hancock CN, Fischer JW. Proline metabolism and cancer: emerging links to glutamine and collagen. Curr Opin Clin Nutr Metab Care 2015;18(1):71–7.

[23] Loayza-Puch F, Rooijers K, Buil LC, Zijlstra J, Oude Vrielink JF, Lopes R, et al. Tumour-specific proline vulnerability uncovered by differential ribosome codon reading. Nature 2016;530(7591):490–4.

[24] Craze ML, Cheung H, Jewa N, Coimbra NDM, Soria D, El-Ansari R, et al. MYC regulation of glutamine-proline regulatory axis is key in luminal B breast cancer. Br J Cancer 2018;118(2):258–65.

[25] Elia I, Broekaert D, Christen S, Boon R, Radaelli E, Orth MF, et al. Proline metabolism supports metastasis formation and could be inhibited to selectively target metastasizing cancer cells. Nat Commun 2017;8:15267.

[26] Phang JM. Proline metabolism in cell regulation and cancer biology: recent advances and hypotheses. Antioxidants Redox Signal 2019;30(4):635–49.

[27] Pavlova NN, Thompson CB. The emerging hallmarks of cancer metabolism. Cell Metabol 2016;23(1):27–47.

[28] Ahn CS, Metallo CM. Mitochondria as biosynthetic factories for cancer proliferation. Cancer Metabol 2015;3.

[29] Loayza-Puch F, Agami R. Monitoring amino acid deficiencies in cancer. Cell Cycle 2016;15(17):2229–30.

[30] Liu W, Hancock CN, Fischer JW, Harman M, Phang JM. Proline biosynthesis augments tumor cell growth and aerobic glycolysis: involvement of pyridine nucleotides. Sci Rep 2015;5:17206.

[31] Pilley SE, Hennequart M, Vandekeere A, Blagih J, Legrave NM, Fendt SM, et al. Loss of attachment promotes proline accumulation and excretion in cancer cells. Sci Adv 2023;9(36):eadh2023.

[32] Zhu GG, Risteli L, Makinen M, Risteli J, Kauppila A, Stenback F. Immunohistochemical study of type I collagen and type I pN-collagen in benign and malignant ovarian neoplasms. Cancer 1995;75(4):1010–7.

[33] Choi J, Credit K, Henderson K, Deverkadra R, He Z, Wiig H, et al. Intraperitoneal immunotherapy for metastatic ovarian carcinoma: resistance of intratumoral collagen to antibody penetration. Clin Cancer Res 2006;12(6):1906–12.

[34] Sherman-Baust CA, Weeraratna AT, Rangel LB, Pizer ES, Cho KR, Schwartz DR, et al. Remodeling of the extracellular matrix through overexpression of collagen VI contributes to cisplatin resistance in ovarian cancer cells. Cancer Cell 2003;3(4):377–86.

[35] Elia I, Rossi M, Stegen S, Broekaert D, Doglioni G, van Gorsel M, et al. Breast cancer cells rely on environmental pyruvate to shape the metastatic niche. Nature 2019;568(7750):117–21.

[36] Bell D, Berchuck A, Birrer M, Chien J, Cramer DW, Dao F, et al. Integrated genomic analyses of ovarian carcinoma. Nature 2011;474(7353):609–15.

[37] Coscia F, Watters KM, Curtis M, Eckert MA, Chiang CY, Tyanova S, et al. Integrative proteomic profiling of ovarian cancer cell lines reveals precursor cell associated proteins and functional status. Nat Commun 2016;7:14.

[38] Livak KJ, Schmittgen TD. Analysis of relative gene expression data using real-time quantitative PCR and the 2(T)(-Delta Delta C) method. Methods 2001;25(4):402–8.

[39] Vincent EE, Sergushichev A, Griss T, Gingras MC, Samborska B, Ntimbane T, et al. Mitochondrial phosphoenolpyruvate carboxykinase regulates metabolic adaptation and enables glucose-independent tumor growth. Mol Cell 2015;60(2):195–207.

[40] Faubert B, Boily G, Izreig S, Griss T, Samborska B, Dong ZF, et al. AMPK is a negative regulator of the warburg effect and suppresses tumor growth in vivo. Cell Metabol 2013;17(1):113–24.

[41] McGuirk S, Gravel S-P, Deblois G, Papadopoli DJ, Faubert B, Wegner A, et al. PGC-1alpha supports glutamine metabolism in breast cancer. Cancer Metabol 2013;1(1). 22-22.

[42] Franken NAP, Rodermond HM, Stap J, Haveman J, van Bree C. Clonogenic assay of cells in vitro. Nat Protoc 2006;1(5):2315–9.

[43] Cerami E, Gao J, Dogrusoz U, Gross BE, Sumer SO, Aksoy BA, et al. The cBio cancer genomics portal: an open platform for exploring multidimensional cancer genomics data. Cancer Discov 2012;2(5):401–4.

[44] Mermel CH, Schumacher SE, Hill B, Meyerson ML, Beroukhim R, Getz G. GISTIC2.0 facilitates sensitive and confident localization of the targets of focal somatic copy-number alteration in human cancers. Genome Biol 2011;12(4):R41.

[45] Coscia F, Watters KM, Curtis M, Eckert MA, Chiang CY, Tyanova S, et al. Integrative proteomic profiling of ovarian cancer cell lines reveals precursor cell associated proteins and functional status. Nat Commun 2016;7.

[46] Vacanti NM, Divakaruni AS, Green CR, Parker SJ, Henry RR, Ciaraldi TP, et al. Regulation of substrate utilization by the mitochondrial pyruvate carrier. Mol Cell 2014;56(3):425–35.

[47] Bricker DK, Taylor EB, Schell JC, Orsak T, Boutron A, Chen YC, et al. A mitochondrial pyruvate carrier required for pyruvate uptake in yeast, Drosophila, and humans. Science 2012;337(6090):96–100.

[48] Hildyard JCW, Ammala C, Dukes ID, Thomson SA, Halestrap AP. Identification and characterisation of a new class of highly specific and potent inhibitors of the mitochondrial pyruvate carrier. Biochim Biophys Acta Bioenerg 2005;1707(2–3):221–30.

[49] Grenell A, Wang Y, Yam M, Swarup A, Dilan TL, Hauer A, et al. Loss of MPC1 reprograms retinal metabolism to impair visual function. Proc Natl Acad Sci U S A 2019;116(9):3530–5.

[50] Du J, Cleghorn WM, Contreras L, Lindsay K, Rountree AM, Chertov AO, et al. Inhibition of mitochondrial pyruvate transport by zaprinast causes massive accumulation of aspartate at the expense of glutamate in the retina. J Biol Chem 2013;288(50):36129–40.

[51] Corbet C, Bastien E, Draoui N, Doix B, Mignion L, Jordan BF, et al. Interruption of lactate uptake by inhibiting mitochondrial pyruvate transport unravels direct antitumor and radiosensitizing effects. Nat Commun 2018;9(1):1208.

[52] Divakaruni AS, Wallace M, Buren C, Martyniuk K, Andreyev AY, Li E, et al. Inhibition of the mitochondrial pyruvate carrier protects from excitotoxic neuronal death. J Cell Biol 2017;216(4):1091–105.

[53] Yang C, Ko B, Hensley CT, Jiang L, Wasti AT, Kim J, et al. Glutamine oxidation maintains the TCA cycle and cell survival during impaired mitochondrial pyruvate transport. Mol Cell 2014;56(3):414–24.

[54] Halestrap AP, Price NT. The proton-linked monocarboxylate transporter (MCT) family: structure, function and regulation. Biochem J 1999;343 Pt 2:281–99.

[55] Ran L, Zhang S, Wang G, Zhao P, Sun J, Zhou J, et al. Mitochondrial pyruvate carrier-mediated metabolism is dispensable for the classical activation of macrophages. Nat Metab 2023;5(5):804–20.

[56] Locasale JW, Grassian AR, Melman T, Lyssiotis CA, Mattaini KR, Bass AJ, et al. Phosphoglycerate dehydrogenase diverts glycolytic flux and contributes to oncogenesis. Nat Genet 2011;43(9):869–74.

[57] DeNicola GM, Chen PH, Mullarky E, Sudderth JA, Hu Z, Wu D, et al. NRF2 regulates serine biosynthesis in non-small cell lung cancer. Nat Genet 2015;47(12):1475–81.

[58] Li AM, Ye J. The PHGDH enigma: do cancer cells only need serine or also a redox modulator? Cancer Lett 2020;476:97–105.

[59] Ying MF, You D, Zhu XB, Cai LM, Zeng SY, Hu X. Lactate and glutamine support NADPH generation in cancer cells under glucose deprived conditions. Redox Biol 2021;46.

[60] Alaqbi SS, Burke L, Guterman I, Green C, West K, Palacios-Gallego R, et al. Increased mitochondrial proline metabolism sustains proliferation and survival of colorectal cancer cells. PLoS One 2022;17(2):e0262364.
[61] Adams E, Frank L. Metabolism of proline and the hydroxyprolines. Annu Rev Biochem 1980;49:1005–61.
[62] Burke L, Guterman I, Palacios Gallego R, Britton RG, Burschowsky D, Tufarelli C, et al. The Janus-like role of proline metabolism in cancer. Cell Death Dis 2020;6:104.
[63] Szlosarek PW, Grimshaw MJ, Wilbanks GD, Hagemann T, Wilson JL, Burke F, et al. Aberrant regulation of argininosuccinate synthetase by TNF-alpha in human epithelial ovarian cancer. Int J Cancer 2007;121(1):6–11.
[64] Cheon DJ, Walts AE, Beach JA, Lester J, Bomalaski JS, Walsh CS, et al. Differential expression of argininosuccinate synthetase in serous and non-serous ovarian carcinomas. J Pathol Clin Res 2015;1(1):41–53.
[65] Eberlin LS, Gabay M, Fan AC, Gouw AM, Tibshirani RJ, Felsher DW, et al. Alteration of the lipid profile in lymphomas induced by MYC overexpression. Proc Natl Acad Sci U S A 2014;111(29):10450–5.
[66] Liu W, Le A, Hancock C, Lane AN, Dang CV, Fan TW, et al. Reprogramming of proline and glutamine metabolism contributes to the proliferative and metabolic responses regulated by oncogenic transcription factor c-MYC. Proc Natl Acad Sci U S A 2012;109(23):8983–8.
[67] Goncalves RLS, Rothschild DE, Quinlan CL, Scott GK, Benz CC, Brand MD. Sources of superoxide/H2O2 during mitochondrial proline oxidation. Redox Biol 2014;2:901–9.
[68] Vettore LA, Westbrook RL, Tennant DA. Proline metabolism and redox; maintaining a balance in health and disease. Amino Acids 2021;53(12):1779–88.
[69] Schworer S, Berisa M, Violante S, Qin WG, Zhu JJ, Hendrickson RC, et al. Proline biosynthesis is a vent for TGF beta-induced mitochondrial redox stress. EMBO J 2020;39(8).
[70] Kuo ML, Bin-Er Lee M, Tang M, den Besten W, Hu SY, Sweredoski MJ, et al. PYCR1 and PYCR2 interact and collaborate with RRM2B to protect cells from overt oxidative stress. Sci Rep 2016;6.
[71] Inoue M. Glutathionists in the battlefield of gamma-glutamyl cycle. Arch Biochem Biophys 2016;595:61–3.
[72] Gamarra Y, Santiago FC, Molina-Lopez J, Castano J, Herrera-Quintana L, Dominguez A, et al. Pyroglutamic acidosis by glutathione regeneration blockage in critical patients with septic shock. Crit Care 2019;23(1):162.
[73] Cheon DJ, Tong YG, Sim MS, Dering J, Berel D, Cui XJ, et al. A collagen-remodeling gene signature regulated by TGF-beta signaling is associated with metastasis and poor survival in serous ovarian cancer. Clin Cancer Res 2014;20(3):711–23.
[74] Yang F, Zhao ZY, Cai SY, Ling L, Hong LY, Tao L, et al. Detailed molecular mechanism and potential drugs for COL1A1 in carboplatin-resistant ovarian cancer. Front Oncol 2021;10.
[75] Wang MY, Wang JJ, Liu JL, Zhu LL, Ma H, Zou J, et al. Systematic prediction of key genes for ovarian cancer by co-expression network analysis. J Cell Mol Med 2020;24(11):6298–307.
[76] Ismail RS, Baldwin RL, Fang J, Browning D, Karlan BY, Gasson JC, et al. Differential gene expression between normal and tumor-derived ovarian epithelial cells. Cancer Res 2000;60(23):6744–9.
[77] Ahmed N, Greening D, Samardzija C, Escalona RM, Chen M, Findlay JK, et al. Unique proteome signature of post-chemotherapy ovarian cancer ascites-derived tumor cells. Sci Rep 2016;6:30061.
[78] Yu P, Fu YX. Targeting tumors with LIGHT to generate metastasis-clearing immunity. Cytokine Growth Factor Rev 2008;19(3–4):285–94.
[79] Siu MK, Kong DS, Chan HY, Wong ES, Ip PP, Jiang L, et al. Paradoxical impact of two folate receptors, FRalpha and RFC, in ovarian cancer: effect on cell proliferation, invasion and clinical outcome. PLoS One 2012;7(11):e47201.
[80] Huang MJ, Zhang W, Wang Q, Yang ZJ, Liao SB, Li L. FOLR1 increases sensitivity to cisplatin treatment in ovarian cancer cells. J Ovarian Res 2018;11(1):15.
[81] Vander Heiden MG, DeBerardinis RJ. Understanding the intersections between metabolism and cancer biology. Cell 2017;168(4):657–69.
[82] Herzig S, Raemy E, Montessuit S, Veuthey JL, Zamboni N, Westermann B, et al. Identification and functional expression of the mitochondrial pyruvate carrier. Science 2012;337(6090):93–6.
[83] Li X, Ji Y, Han G, Li X, Fan Z, Li Y, et al. MPC1 and MPC2 expressions are associated with favorable clinical outcomes in prostate cancer. BMC Cancer 2016;16(1):894.
[84] Bader DA, Hartig SM, Putluri V, Foley C, Hamilton MP, Smith EA, et al. Mitochondrial pyruvate import is a metabolic vulnerability in androgen receptor-driven prostate cancer. Nat Metab 2019;1(1):70–85.
[85] Zou H, Chen Q, Zhang A, Wang S, Wu H, Yuan Y, et al. MPC1 deficiency accelerates lung adenocarcinoma progression through the STAT3 pathway. Cell Death Dis 2019;10(3):148.
[86] You JH, Lee J, Roh JL. Mitochondrial pyruvate carrier 1 regulates ferroptosis in drug-tolerant persister head and neck cancer cells via epithelial-mesenchymal transition. Cancer Lett 2021;507:40–54.
[87] Nagampalli RSK, Quesnay JEN, Adamoski D, Islam Z, Birch J, Sebinelli HG, et al. Human mitochondrial pyruvate carrier 2 as an autonomous membrane transporter. Sci Rep 2018;8(1):3510.
[88] Compan V, Pierredon S, Vanderperre B, Krznar P, Marchiq I, Zamboni N, et al. Monitoring mitochondrial pyruvate carrier activity in real time using a BRET-based biosensor: investigation of the warburg effect. Mol Cell 2015;59(3):491–501.
[89] Sullivan LB, Luengo A, Danai LV, Bush LN, Diehl FF, Hosios AM, et al. Aspartate is an endogenous metabolic limitation for tumour growth. Nat Cell Biol 2018;20(7):782–8.
[90] Garcia-Bermudez J, Baudrier L, La K, Zhu XG, Fidelin J, Sviderskiy VO, et al. Aspartate is a limiting metabolite for cancer cell proliferation under hypoxia and in tumours (vol 20, pg 775, 2018). Nat Cell Biol 2018;20(10). 1228-1228.
[91] Birsoy K, Wang T, Chen WW, Freinkman E, Abu-Remaileh M, Sabatini DM. An essential role of the mitochondrial electron transport chain in cell proliferation is to enable aspartate synthesis. Cell 2015;162(3):540–51.
[92] Schell JC, Olson KA, Jiang L, Hawkins AJ, Van Vranken JG, Xie J, et al. A role for the mitochondrial pyruvate carrier as a repressor of the Warburg effect and colon cancer cell growth. Mol Cell 2014;56(3):400–13.
[93] Westbrook RL, Bridges E, Roberts J, Escribano-Gonzalez C, Eales KL, Vettore LA, et al. Proline synthesis through PYCR1 is required to support cancer cell proliferation and survival in oxygen-limiting conditions. Cell Rep 2022;38(5):110320.
[94] Hollinshead KER, Munford H, Eales KL, Bardella C, Li C, Escribano-Gonzalez C, et al. Oncogenic IDH1 mutations promote enhanced proline synthesis through PYCR1 to support the maintenance of mitochondrial redox homeostasis. Cell Rep 2018;22(12):3107–14.
[95] Kabel M, Madore J, Ramus SJ, Clarke BA, Pharoah PDP, Deen S, et al. Evidence for a time-dependent association between FOLR1 expression and survival from ovarian carcinoma: implications for clinical testing. An Ovarian Tumour Tissue Analysis consortium study. Br J Cancer 2014;111(12):2297–307.
[96] Tang L, Zeng J, Geng P, Fang C, Wang Y, Sun M, et al. Global metabolic profiling identifies a pivotal role of proline and hydroxyproline metabolism in supporting hypoxic response in hepatocellular carcinoma. Clin Cancer Res 2018;24(2):474–85.
[97] Sun C, Li T, Song X, Huang L, Zang Q, Xu J, et al. Spatially resolved metabolomics to discover tumor-associated metabolic alterations. Proc Natl Acad Sci U S A 2019;116(1):52–7.
[98] Gao Q, Zhu H, Dong L, Shi W, Chen R, Song Z, et al. Integrated proteogenomic characterization of HBV-related hepatocellular carcinoma. Cell 2019;179(2):561–577 e522.
[99] Nakayama T, Al-Maawali A, El-Quessny M, Rajab A, Khalil S, Stoler JM, et al. Mutations in PYCR2, encoding pyrroline-5-carboxylate reductase 2, cause microcephaly and hypomyelination. Am J Hum Genet 2015;96(5):709–19.

[100] Tothill RW, Tinker AV, George J, Brown R, Fox SB, Lade S, et al. Novel molecular subtypes of serous and endometrioid ovarian cancer linked to clinical outcome. Clin Cancer Res 2008;14(16):5198—208.

[101] Cancer Genome Atlas Research N. Integrated genomic analyses of ovarian carcinoma. Nature 2011;474(7353):609—15.

[102] Sethi T, Rintoul RC, Moore SM, MacKinnon AC, Salter D, Choo C, et al. Extracellular matrix proteins protect small cell lung cancer cells against apoptosis: a mechanism for small cell lung cancer growth and drug resistance in vivo. Nat Med 1999;5(6):662—8.

[103] Lamande SR, Morgelin M, Adams NE, Selan C, Allen JM. The C5 domain of the collagen VI alpha3(VI) chain is critical for extracellular microfibril formation and is present in the extracellular matrix of cultured cells. J Biol Chem 2006;281(24):16607—14.

[104] Aigner T, Hambach L, Soder S, Schlotzer-Schrehardt U, Poschl E. The C5 domain of Col6A3 is cleaved off from the Col6 fibrils immediately after secretion. Biochem Biophys Res Commun 2002;290(2):743—8.

[105] Park J, Scherer PE. Adipocyte-derived endotrophin promotes malignant tumor progression. J Clin Invest 2012;122(11):4243—56.

[106] Ohlund D, Lundin C, Ardnor B, Oman M, Naredi P, Sund M. Type IV collagen is a tumour stroma-derived biomarker for pancreas cancer. Br J Cancer 2009;101(1):91—7.

[107] Mazouni C, Arun B, Andre F, Ayers M, Krishnamurthy S, Wang B, et al. Collagen IV levels are elevated in the serum of patients with primary breast cancer compared to healthy volunteers. Br J Cancer 2008;99(1):68—71.

